

SPECTRAL ALBEDO AND EMISSIVITY OF CO₂ IN MARTIAN POLAR CAPS:
MODEL RESULTS

Stephen G. Warren¹

Glaciology Section, Antarctic Division, University of Melbourne, Australia

Warren J. Wiscombe

NASA Goddard Space Flight Center, Greenbelt, Maryland

John F. Firestone

Geophysics Program, University of Washington, Seattle, Washington

Abstract. A model originally developed to explain the spectral albedo and emissivity of terrestrial snow is extended to the case of carbon dioxide snow on Mars. The variation of albedo and emissivity with wavelength is caused by the spectral variation of the absorption coefficient of solid CO₂. The most important variables controlling the radiative properties are grain size and contamination by dust or water. Solar zenith angle and snowpack thickness are of less importance. The observation that red albedo is higher than blue albedo in the Martian south polar cap indicates that the snow is contaminated with red dust. The interband absorption coefficient of CO₂ ice in the thermal infrared is 2-3 orders of magnitude smaller than that of H₂O ice, due to the absence of hydrogen bonding in CO₂. This allows CO₂ snow emissivity to be sensitive to grain size, emission angle, and impurities, in contrast to water snow which is nearly a blackbody under all conditions. The emissivity of CO₂ snow varies substantially with wavelength, so energy budget modeling should be done in spectral detail. The addition of a thin layer of water frost over CO₂ snow dramatically raises the thermal emissivity but causes little change to the spectrally averaged albedo unless the underlying CO₂ snow is dirty. Remote sensing of CO₂ grain size, H₂O content, and dust content may be possible. However, the design of a remote-sensing strategy awaits more accurate laboratory determination of the optical constants of CO₂ ice.

Polar Caps of Mars

The polar caps of Mars undergo dramatic seasonal changes. The south cap, for example, advances to 40°-45°S in winter, retreating to 85°S in summer [Briggs et al., 1977; James et al., 1979]. Atmospheric pressure variations measured by Viking landers, as well as infrared temperatures measured by Viking orbiters, indicate that these seasonal caps are composed of solid carbon dioxide. Photographic

evidence of wind-drifted material, as well as the high reflectivity for visible light, indicates that this solid CO₂ is made up of small particles, like snow on Earth. It may form in the atmosphere by nucleating around small dust particles or H₂O crystals, or it may be deposited directly onto the surface as frost. The average depth of this snow layer has been estimated, from the seasonal cycle of atmospheric pressure at the Viking lander sites, to be a few tens of centimeters [Hess et al., 1979]. The CO₂ snow is probably mixed with wind-blown dust from the red Martian soil [Toon et al., 1980] and with small amounts of H₂O ice [Kieffer, 1968, 1990].

In order to help understand the Martian radiation budget and to help interpret Mariner and Viking measurements of solar and infrared radiation from the polar caps, we use a radiative transfer model to calculate the spectral albedo and emissivity of CO₂ snow from the ultraviolet to the thermal infrared. We examine the influence of snow grain sizes, snow layer thickness, solar zenith angle or infrared emission angle, and dust or water content. These model predictions, however, are only tentative because of our imprecise knowledge of the complex refractive index of CO₂ ice.

We have no direct Martian surface measurements against which to compare our model. The spectral radiances measured by Mariner and Viking refer to the surface and atmosphere combined, and furthermore they are intensities, not fluxes as our model predicts. It may be difficult to infer surface properties from the Viking measurements, because of the unknown and variable optical thicknesses of dust clouds and ice clouds in the Martian polar atmosphere. Even small optical depths of dust can significantly lower the planetary albedo over a bright surface [Davies, 1979, Figure 1].

There are, however, some laboratory measurements of the reflectance of CO₂ frost. Kieffer [1968, 1970] measured bidirectional reflectance for wavelengths 0.8-3.2 μm. He raised a number of issues which we also address in this paper, namely, the effect of grain size, the nonunit emissivities, H₂O contamination in small amounts, angular dependence, and the depth necessary for CO₂ snow to be effectively semi-infinite.

Polar cap albedo and emissivity seem to have great influences on the climate of Mars. The energy budget of the polar regions is dominated by radiative fluxes [Paige and Ingersoll, 1985]. The energy balance climate model of James and North [1982] predicted that the formation of the seasonal CO₂ ice caps is very sensitive to longwave emissivity ϵ , with the total CO₂ condensation being roughly pro-

¹Now at Geophysics Program, University of Washington, Seattle, Washington.

portional to ϵ . The best fit of their model to the seasonal surface pressure variation in the non-dust-storm period, as observed by the Viking landers, was obtained by assuming $\epsilon=0.57$ and planetary albedo=0.75 over the poles.

The visible wavelength planetary albedos over the south polar cap measured from Viking [James et al., 1979] scatter widely, probably due not only to variable dust content but also to variable fraction of bare ground within the field of view. The highest blue ($\lambda=0.45 \mu\text{m}$) albedos were 0.3-0.4, with corresponding "red" ($\lambda=0.59 \mu\text{m}$) albedos of 0.5-0.6. (These albedos were computed using an empirical bidirectional reflectance function obtained by viewing the same region from different aspects.)

The broadband (0.3-3 μm) albedos of the south polar cap from Viking were discussed in detail by Kieffer [1979]. He found albedos in the range 0.35-0.50, not large enough to achieve radiation balance. The albedos were highest near the cap edge in spring but highest near the pole during summer. Paige and Ingersoll [1985], however, reanalyzed these data, developing an empirical bidirectional reflectance distribution function, and obtained south polar cap planetary albedos of 0.55-0.75, averaging about 0.65 over the entire Martian spring and summer seasons.

Infrared emission was measured by Viking's infrared thermal mapper (IRTM) in five spectral channels. The four centered at 7, 9, 11, and 20 μm (in spectral regions of weak atmospheric absorption) should, in the absence of clouds, sense the surface temperature. Unlike bare ground and the summertime H₂O-ice cap at the north pole, where the brightness temperatures T₇, T₉, T₁₁, and T₂₀ all agreed, at the CO₂-ice-covered wintertime south pole these four temperatures disagreed by up to 45 K. This is illustrated well in Figures 2a and 3a of Paige and Ingersoll [1985]. Kieffer [1979] ascribed these differences in brightness temperature to a combination of atmospheric dust, dark warm patches in the cap, and low 20- μm emissivity of CO₂. Many of the brightness temperatures are significantly in excess of 150 K, the CO₂ sublimation temperature at the 6-mbar pressure level. These higher temperatures were attributed by Kieffer [1979] to dust in the warm atmosphere and to warm sub-grid-scale frost-free surfaces adjacent to CO₂ ice surfaces at 150 K.

There is apparently considerable variation in temperature or emissivity or both across the south polar cap. Figure 6 of Kieffer et al. [1977] shows that in midwinter T₂₀ varied from 148 K near the edge of the polar cap to 130 K at the south pole. Assuming that the entire ice cap surface consists of solid CO₂ at 150 K, these values of T₂₀ imply that the surface emissivity varies from near 1.0 at the edge of the cap to 0.5 at the pole (presuming no atmospheric emission, which is an oversimplification). The average T₂₀ was 143 K, which could be explained by an emissivity of 0.8. However, the physical temperature may have been somewhat lower at the pole, due to enrichment of the minor atmospheric gases and local lowering of the sublimation temperature [Kieffer et al., 1976].

Most planetary surfaces have emissivities above 90% in the thermal infrared. In particular, this is true for snow and sea ice on Earth, which have emissivity about 99% for practically any grain size and snowpack thickness (Dozier and Warren [1982]; reviewed below). But the above evidence suggests that CO₂ is an anomalous planetary surface, having quite variable surface emissivity. We will show that the reason for the difference in emissivity between H₂O snow and CO₂ snow is that the interband absorption coefficient of CO₂ ice in the infrared is 2-3 orders of

magnitude smaller than that of H₂O ice, apparently because of the lack of hydrogen bonding in CO₂ ice.

In this paper we often contrast the properties of water snow and CO₂ snow, because both occur on Mars. Kieffer [1968] suggested that H₂O frost may sometimes cover a CO₂ snow surface and dominate the reflectance properties. Also, the north polar cap in summer consists of H₂O ice.

Snow Albedo/Emissivity Model

Our model for the spectral albedo of terrestrial water snow [Wiscombe and Warren, 1980] (hereinafter referred to as WWI) should also be useful for CO₂ snow. This model uses Mie theory for the single scattering by individual snow grains, together with the delta-Eddington method [Joseph et al., 1976] for the multiple scattering in a snowpack. In spite of the far-field limit taken in Mie theory, the model agrees quite well with measured spectral albedos even for closely packed snow [Warren et al., 1986], provided that the particle sizes and spaces between particles are large compared to the wavelength of light. This condition is satisfied for solar radiation but may break down in the thermal infrared if snow particles are small (grain radius $r < 50 \mu\text{m}$). It is possible to incorporate near-field effects into the model.

The single-scattering calculation is done for spheres, so we assume that we can mimic the albedo of a snowpack of nonspherical particles by a model snowpack of "equivalent" spheres. When the particle size is much larger than the wavelength, which is generally true for water snow in the solar and thermal-infrared spectral regions, the equivalent sphere seems to be best chosen as the sphere with the same surface-to-volume ratio as the real nonspherical snow grain [Dobbins and Jizmagian, 1966; Kieffer, 1968; Warren, 1982]. This is because what largely controls the albedo is the average distance a light ray travels through ice between air-ice interfaces, i.e., between opportunities for changing direction. That is also the reason that a coarse-grained snowpack is more absorptive than a fine-grained snowpack, as shown below.

The single-scattering calculation at a particular wavelength λ requires as input (1) the size parameter $x = 2\pi r/\lambda$, i.e., the ratio of the particle's circumference to the wavelength; and (2) the complex index of refraction m at that wavelength; $m = m_{re} - i m_{im}$, where m_{re} is the ordinary refractive index which determines the phase speed and m_{im} is related to the linear absorption coefficient (k_{abs} , units of inverse length) as $k_{abs} = 4\pi m_{im}/\lambda$ (m_{re} and m_{im} are together called the optical constants). The single-scattering calculation follows Mie theory, using the algorithm of Wiscombe [1980] or (for $x > 2000$) the asymptotic formulae of Nussenzveig and Wiscombe [1980].

The results of the Mie calculation are single-scattering albedo $\tilde{\omega}$ (the probability that a photon will survive an extinction event), the extinction efficiency Q_{ext} (ratio of the extinction cross section of a particle to its geometric cross-section area), and the scattering phase function, which describes the angular distribution of the photons scattered by a single particle. The radiative transfer method that we use, delta-Eddington, requires only one measure of the phase function, the average value of the cosine of the scattering angle, called the asymmetry parameter g .

The analytical formula for albedo, a , for parallel-beam incidence is given by equations 3 and 4 of WWI. It depends on $\tilde{\omega}$, g , and the cosine μ_0 of the solar zenith angle θ_0 and (for a thin snowpack only) on Q_{ext} , the snowpack thickness

and the albedo of the underlying surface. The albedo for diffuse incidence is obtained by integrating the direct beam albedo over all incidence angles in the hemisphere (equations 6 and 7 of WWI).

On Mars the spectrum of thermal ("longwave") radiation is well separated from the spectrum of solar ("shortwave") radiation energy, even more so than on Earth. For a typical Martian temperature of 195 K the emitted and incident spectral fluxes are approximately equal (and small) at $\lambda=6\ \mu\text{m}$, so beyond $6\ \mu\text{m}$ the quantity of interest is the emissivity rather than the albedo. For an opaque surface, albedo and emissivity must add to unity, by Kirchhoff's law [Siegel and Howell, 1972, p. 70]:

$$\varepsilon(\theta, \lambda) = 1 - a(\theta, \lambda)$$

where $\varepsilon(\theta, \lambda)$ is the directional emissivity at wavelength λ into the viewing zenith angle θ , and $a(\theta, \lambda)$ is the albedo for a direct beam coming from zenith angle θ . To compute the emissivity, we therefore just compute the albedo and subtract it from unity.

Optical Constants

CO₂ Ice

Laboratory measurements of the absorption spectrum of pure solid CO₂ were reviewed by Warren [1986], who also compiled a set of recommended values for radiation modeling, which we use in this paper. However, there are considerable uncertainties in that compilation, in nearly all spectral regions except the strong absorption bands at $4\text{-}\mu\text{m}$ and $15\text{-}\mu\text{m}$ wavelength. The near-infrared region, $1.0\text{-}2.5\ \mu\text{m}$, has never been measured. The visible and near-visible, $0.3\text{-}1.0\ \mu\text{m}$, was measured by Egan and Spagnolo [1969], but they used unpurified commercial dry ice, so we cannot rule out the presence of trace amounts of an absorptive impurity.

Spectral transmittance for the infrared region, $2.5\text{-}25\ \mu\text{m}$, was measured by Diteon and Kieffer [1979], but their crystals were poorly formed and probably scattered as much light as they absorbed. The amount of scattering has been estimated [Diteon and Kieffer, 1979; Warren, 1986], but it is quite uncertain, so the optical constants in this spectral region are correspondingly uncertain.

The spectrum has never been measured beyond $25\text{-}\mu\text{m}$ wavelength, so our computations of CO₂ snow emissivity also stop there. However, we do compute albedo in the region $1.0\text{-}2.5\ \mu\text{m}$, using optical constants guessed by extrapolation of m_{im} from the region $0.3\text{-}1.0\ \mu\text{m}$.

H₂O ice

The laboratory measurements of the absorption spectrum of water ice were reviewed by Warren [1984]; we use that compilation in this paper. These differ slightly from those used by WWI, because we now have available the more recent accurate determination of m_{im} by Grenfell and Perovich [1981] for $0.4\text{-}1.4\ \mu\text{m}$ wavelength. Our graphs of water snow albedo thus differ slightly from those in WWI.

Martian Dust

For our calculations of the albedo and emissivity of snow containing Martian dust, we use dust optical constants recommended by Pollack et al. [1979] in the spectral regions where they inferred them. For wavelengths

$0.4\text{-}1.1\ \mu\text{m}$, we took the values of m_{im} from Figure 11 of Pollack et al. [1977] and reduced them by a factor of 10 as recommended by Pollack et al. [1979]. (Pollack [1982] discussed how the values of m_{im} were estimated by analysis of the spectral sky brightness seen from a Viking lander.) For $0.35\text{-}0.4\ \mu\text{m}$ we extrapolated the trend of $m_{\text{im}}(\lambda)$ from $\lambda > 0.4\ \mu\text{m}$. The real index we assumed constant, $m_{\text{re}}=1.55$, for $0.35\text{-}1.1\ \mu\text{m}$.

For $5\text{-}40\ \mu\text{m}$, the dust optical constants recommended by Pollack et al. [1979] were those measured by Toon et al. [1977] for montmorillonite sample 219b. For the gap in data from 1.1 to $5\ \mu\text{m}$, we refer to Grim [1953]. His plots (Figure 115) of transmission versus wavelength for five montmorillonite samples imply that m_{im} is approximately constant from 2 to $6\ \mu\text{m}$. Toon et al. used a reflection method to obtain m_{im} , which is unreliable when $m_{\text{im}} \ll 0.1$. We thus ignore their values between 5 and $6.25\ \mu\text{m}$ and simply interpolate m from $1.1\ \mu\text{m}$ ($m = 1.55 - 0.01i$) to $6.25\ \mu\text{m}$ ($m = 1.32 - 0.01i$). This gives us the desired constancy of m_{im} in this spectral region.

Single-Scattering Quantities for CO₂ Ice Particles

Many of our figures are in four parts. Parts a and b show the spectral region of solar energy, $0.2\text{-}1.6\ \mu\text{m}$ and $1.6\text{-}6.0\ \mu\text{m}$. Part c shows the part of the thermal infrared region for which we have optical constants for CO₂ ice, i.e., $6\text{-}25\ \mu\text{m}$. There is often considerable variation of radiative properties in the neighborhood of the sharp absorption lines characteristic of the CO₂ ice spectrum, which is difficult to display and is not resolved in parts a-c of the figures, but most of these lines cover only an extremely small spectral range. The most important such region, both for remote sensing and for the energy budget, is the $15\text{-}\mu\text{m}$ band, so we expand this region in part d. The thermal infrared figures c and d are drawn with both wavelength and wave number scales.

Figures 1-3 plot Q_{ext} , $\tilde{\omega}$, and g for CO₂ ice spheres of radii $r=10, 100, \text{ and } 1000\ \mu\text{m}$. Q_{ext} (Figure 1) is close to its geometric optics limit of 2.0 for $r=100$ and $1000\ \mu\text{m}$, even in the bands at 4 and $15\ \mu\text{m}$. The $10\text{-}\mu\text{m}$ particle exhibits a resonance peak in Q_{ext} at $\lambda \approx 2r$ (interrupted by the $15\text{-}\mu\text{m}$ band).

The wavelength dependence of single-scattering coalbedo ($1-\tilde{\omega}$) shown in Figure 2 parallels that of m_{im} . It increases with grain size at all wavelengths, except in the strong absorption bands. This means that large particles are more absorptive than small particles, for all particles in the range of interest for CO₂ snow. (The contrary finding by Hunt et al. [1980] that $(1-\tilde{\omega})$ decreases with increasing particle size is true only for very small particles, i.e., for $r < 0.1\ \mu\text{m}$ at $\lambda=0.35\ \mu\text{m}$ or $r < 10\ \mu\text{m}$ at $\lambda=30\ \mu\text{m}$.) The sharp spikes at 1.4 and $2.0\ \mu\text{m}$ are due to very narrow absorption lines [Warren, 1986] which are not resolved in these figures. Because the optical constants are not established in the region $1.0\text{-}2.5\ \mu\text{m}$, there are likely to be other absorption features yet to be discovered. T. Z. Martin (Mariner 7 IR spectra of the Martian south polar cap, submitted to *Journal of Geophysical Research*, 1989) has found features in infrared spectra of the Martian south polar cap which do not appear in our graphs.

The asymmetry parameter g (Figure 3), which can assume values from +1 (total forward scattering) to -1 (total backscattering), is generally greater than 0.8 for the larger particles, outside the strong absorption bands. The asymmetry parameter increases as r increases. These large values of

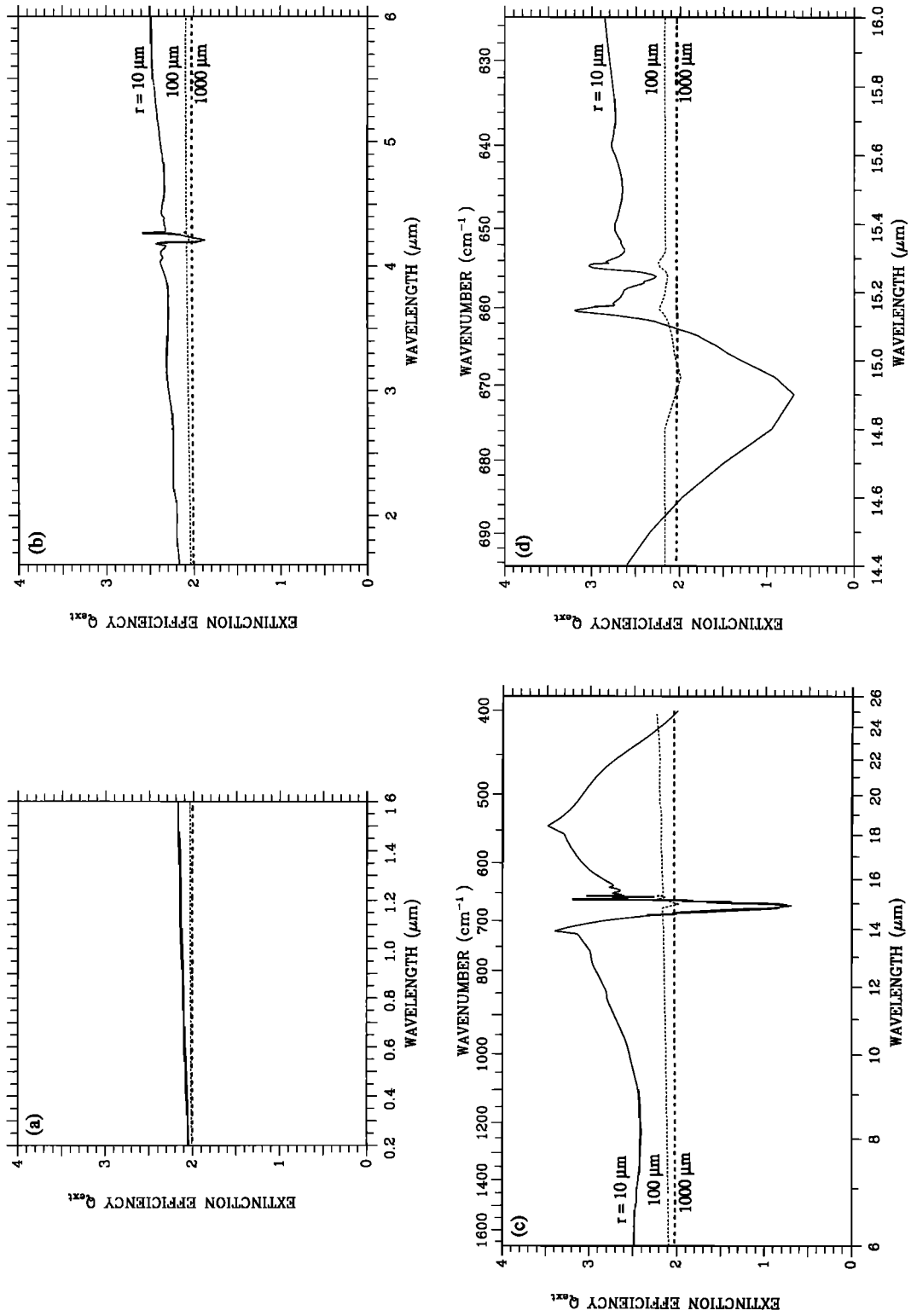


Fig. 1. Extinction efficiency Q_{ext} for CO₂ ice spheres of various radii, as a function of wavelength.

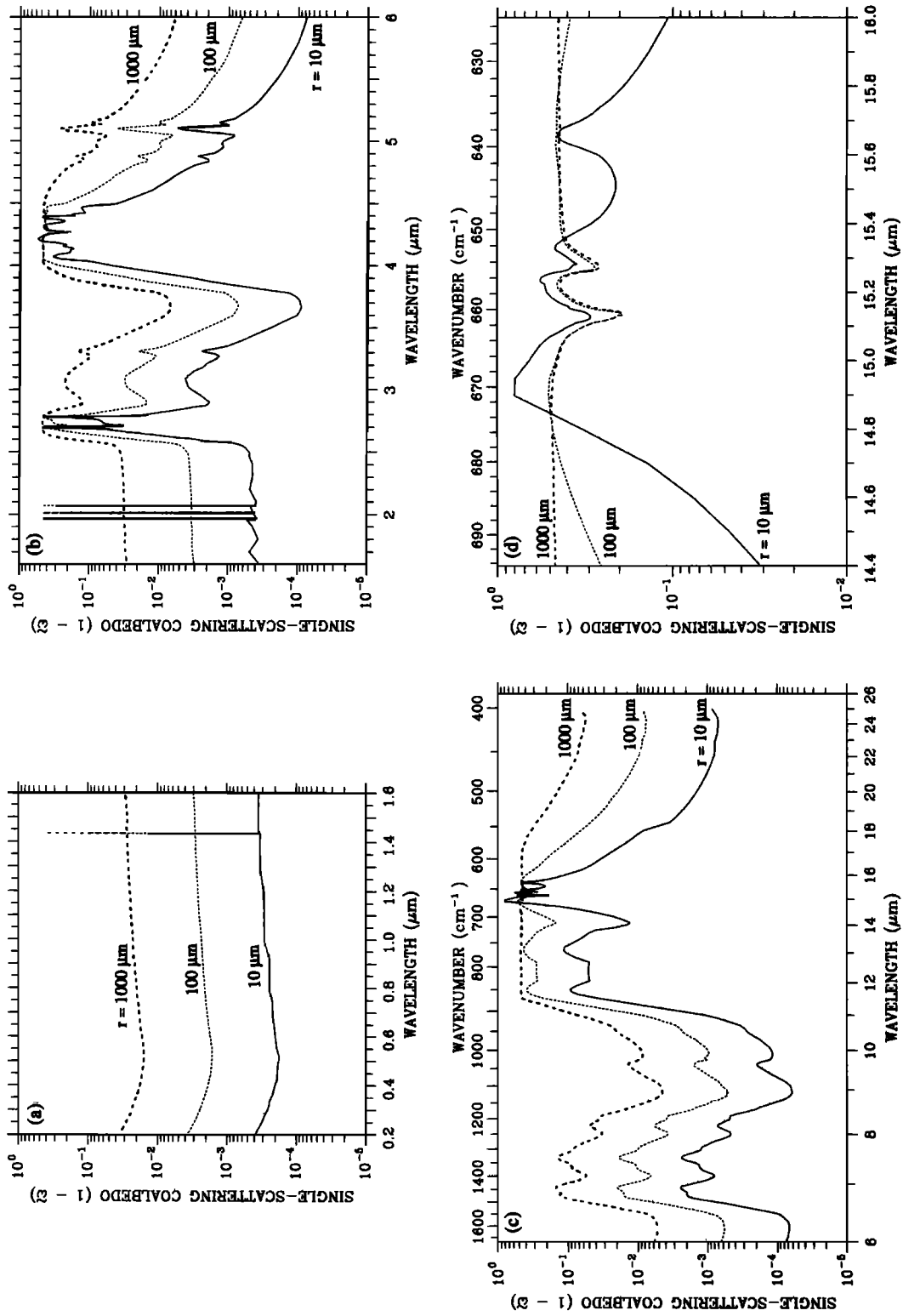


Fig. 2. Single-scattering coaledbedo (1 - $\bar{\omega}$) for CO₂ ice spheres of various radii, as a function of wavelength.

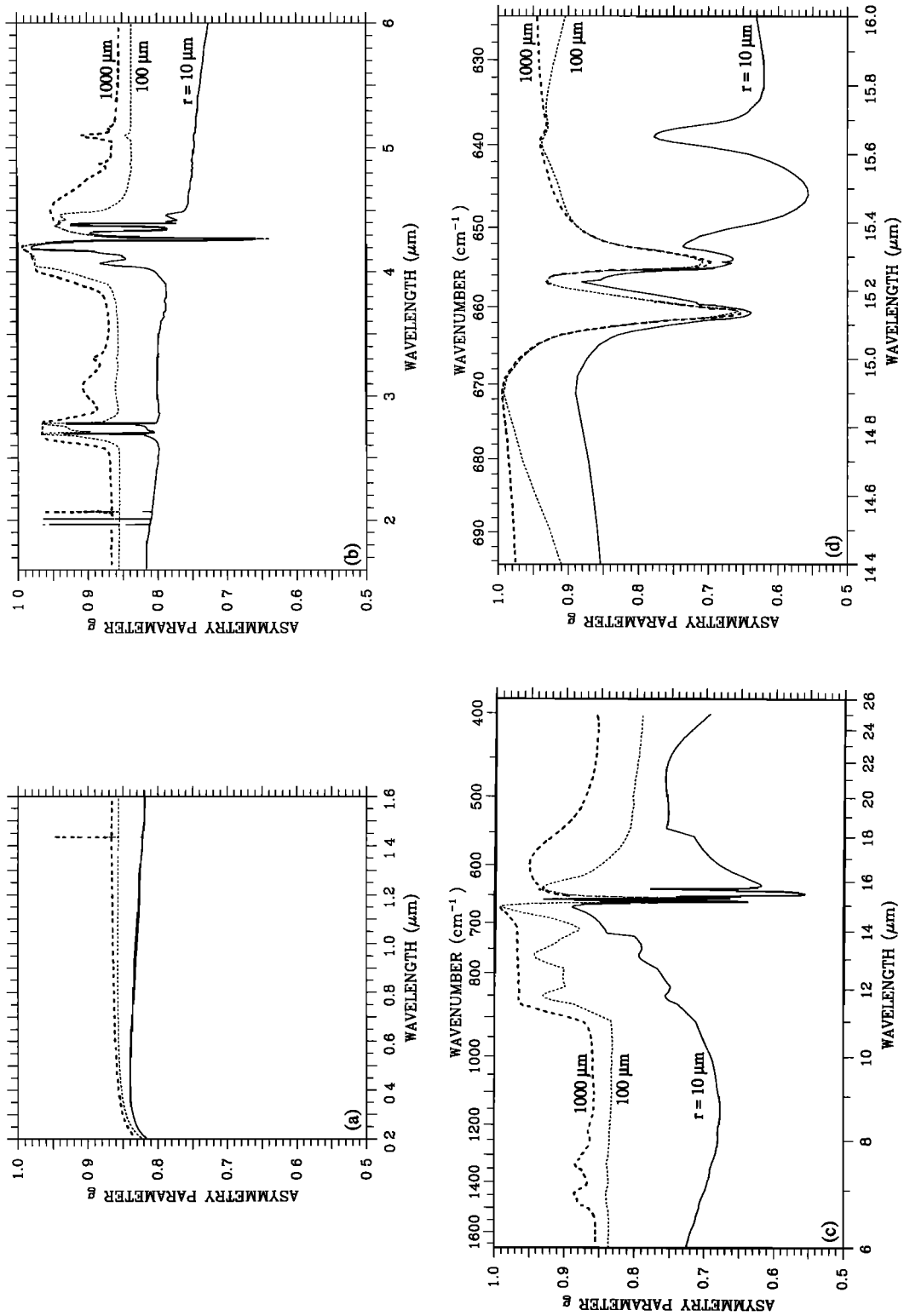


Fig. 3. Asymmetry parameter g for CO₂ ice spheres of various radii, as a function of wavelength.

g indicate strongly forward directed scattering, which is mainly due to a very narrow forward peak in the scattering phase function representing photons that diffract around the particle and change their direction only slightly. In order to calculate fluxes accurately from a medium with $g > 0.5$, a multiple-scattering method such as delta-Eddington is appropriate, which approximates a fraction of the slightly deflected photons as being unscattered, and transforms the radiative transfer problem into an equivalent one with $g < 0.5$ [Joseph et al., 1976].

Effect of Snow Grain Size on Albedo and Emissivity

The wavelength dependence of albedo or emissivity is determined by the wavelength dependence of m_{im} . At any particular wavelength, however, the most important variable controlling the albedo is the snow grain size. As mentioned

above, the "equivalent sphere" for an irregular snow particle is likely to be the one with the same surface-to-volume ratio. Nonsphericity becomes less important in situations with considerable multiple scattering, so its effects are unlikely to be detected for snow except in the angular distribution of reflected intensity for near-grazing angles of incidence.

Albedo of Water Snow

For terrestrial water snow we found that in order to match field observations of spectral albedo, the radii of the equivalent spheres ranged from 50 μm for new snow to 1000 μm for old melting snow. This also corresponds to photographic and microscopic measurements of snow grain size. Figure 4 shows the calculated albedo of water snow for grain sizes in this range. The grain size normally increases

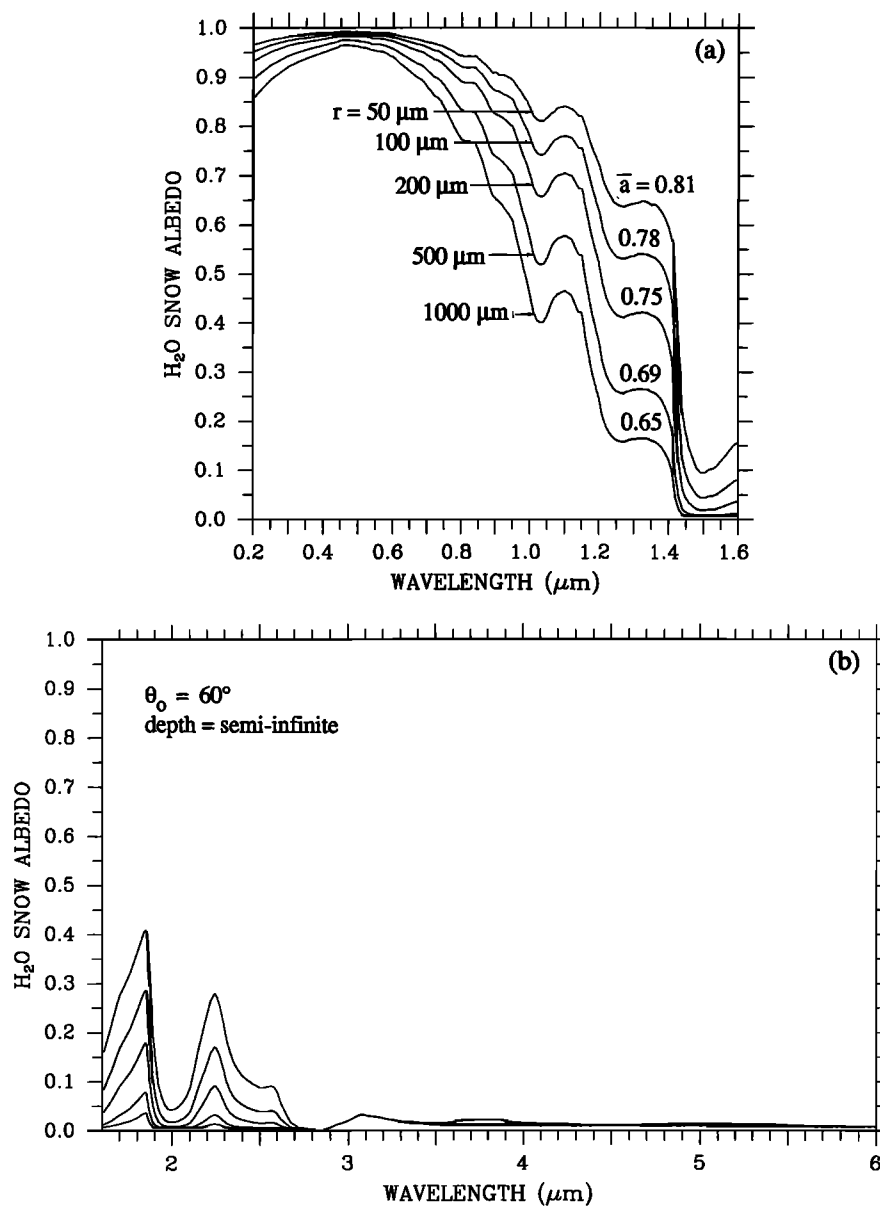


Fig. 4. Model-calculated spectral albedo of water snow, for various snow grain radii, at zenith angle $\theta_0=60^\circ$. (From Figure 8 of Wiscombe and Warren [1980], but using revised values of optical constants of ice from Warren [1984].) Spectrally averaged albedos \bar{a} are also given, computed by equation (1).

as the snow ages due to "destructive metamorphism" [LaChapelle, 1969]. For wind-blown snow on Earth's antarctic plateau, where the grains are nearly spherical, the measured grain radii (50-100 μm) agree rather well with the optical grain size necessary to explain albedo measurements there (T. C. Grenfell et al., manuscript in preparation, 1990).

The albedo is high in the visible and rather insensitive to grain size but drops to low values in the near-infrared. The region most sensitive to grain size is 0.8-2.4 μm, so these are the wavelengths most useful for remote sensing of grain size and for discrimination of snow from clouds (which have even smaller particle sizes).

The spectrally averaged albedo \bar{a} is also given on the curves:

$$\bar{a} = \frac{\int S(\lambda)a(\lambda)d\lambda}{\int S(\lambda)d\lambda} \quad (1)$$

where $S(\lambda)$ is the spectral distribution of solar energy. $S(\lambda)$

varies with cloud thickness, oxygen amount, and ozone amount, so it is different at the surface of Mars than at the Earth's surface. For computing \bar{a} in this paper, we just use the top-of-atmosphere values of $S(\lambda)$. The limits of integration are 0.2 μm (the lower limit for significant solar radiation at the Martian surface), and 6.0 μm (the wavelength at which the incident shortwave and emitted longwave spectral fluxes are equal for a blackbody surface at 195 K on Mars).

Albedo of CO₂ Snow

The calculated albedo of CO₂ snow (Figure 5) may be contrasted with that of H₂O snow (Figure 4). Since we do not know the grain sizes of CO₂ snow, we have used the range of H₂O snow grain size as a guide but have also carried out calculations for both larger and smaller grains. The curves in Figure 5 (and other figures below) are dashed in regions where m_{im} is uncertain by more than a factor of 10 to indicate that the albedo is also highly uncertain.

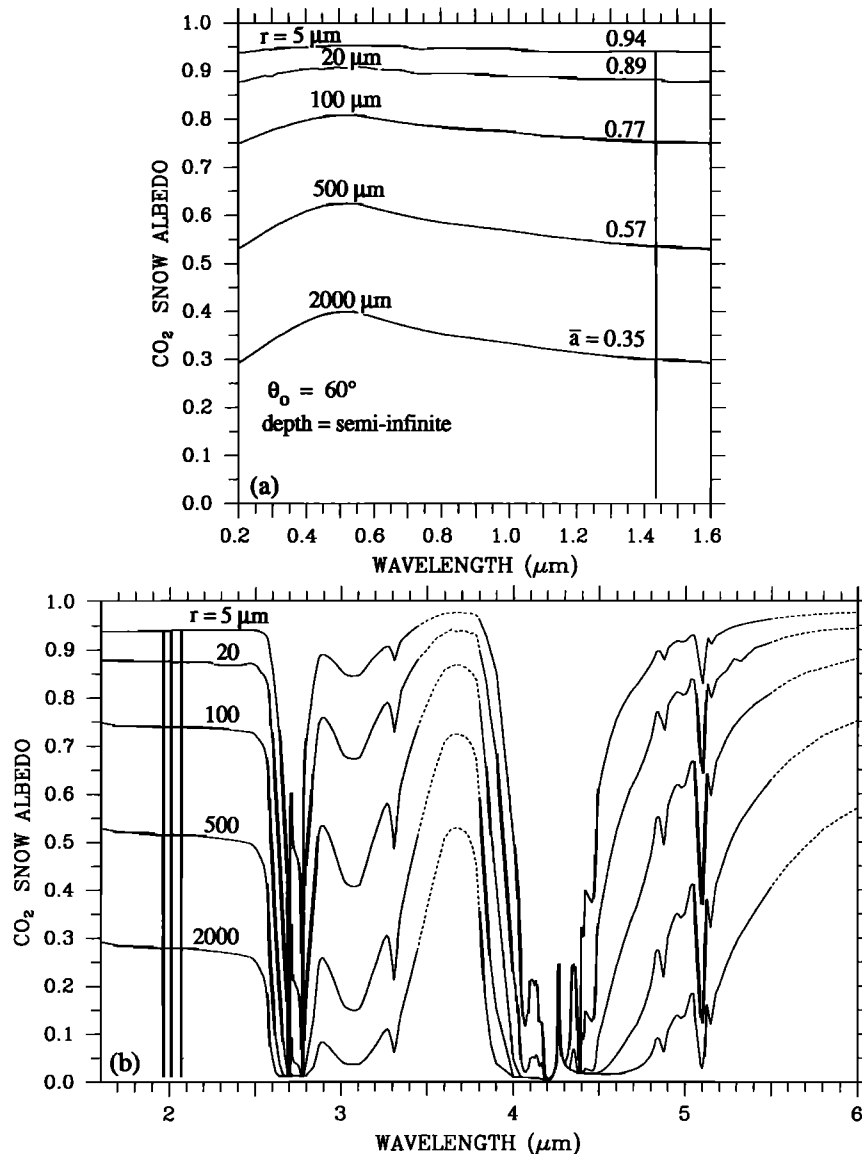


Fig. 5. Spectral albedo of CO₂ snow, at zenith angle $\theta_0=60^\circ$, calculated for various grain radii. Spectrally averaged albedo \bar{a} is also given. Dashed curves are drawn for spectral regions where the imaginary refractive index is uncertain by more than a factor of 10.

Based on atmospheric CO₂ advection rates, estimated dust particle concentrations, and the assumption that CO₂ snow nucleates on dust particles, Pollack et al. [1977] estimated an average radius of 25 μm for CO₂ snow. However, one must distinguish the average radius \bar{r} from the optically effective radius r_{eff} of an ensemble of particles with size distribution $N(r)$:

$$\bar{r} = \int rN(r)dr / \int N(r)dr$$

whereas
$$r_{\text{eff}} = \int r^3N(r)dr / \int r^2N(r)dr$$

so r_{eff} is always larger than \bar{r} . Hansen and Travis [1974] showed that r_{eff} (which is a surface-area-weighted mean radius) was usually sufficient to predict the radiative properties of a cloud, whatever the shape of the size distribution. The radius estimated by Pollack et al. is probably closer to \bar{r} .

The evidence of drifting snow in the south polar region [Thomas et al., 1979] can suggest upper limits to the grain sizes if the wind speeds are known. Iversen et al. [1976] and Pollack et al. [1976] found the friction velocities implied by the geostrophic winds to be only marginally adequate to move snow particles of any size. There is an optimum particle size for suspension by wind, which is between 50- and 200-μm radius, depending on the assumed atmospheric stability, pressure, roughness height, and other parameters.

In the absence of more direct measurements of grain sizes, we have calculated albedo and emissivity for grain radii from 5 to 2000 μm. We use $r=100$ μm as the standard grain size for investigation of the effects of zenith angle, depth, and contamination.

The spectral albedo in Figure 5 is calculated for a "semi-infinite" snowpack (i.e., thick enough that negligible radiation energy reaches the underlying surface) and for a direct solar beam at a zenith angle of 60°, typical of noon in mid-latitude winter or subpolar spring and summer (because the tilt of Mars' axis is 25°). This zenith angle is also close to the "effective" zenith angle of isotropic diffuse radiation (WWI), so Figure 5 will also apply under a sufficiently thick cloud.

The albedo decreases with increasing grain size. This is due in small part to the increase of g with r but mainly to the increase of $(1-\tilde{\omega})$ with r . For radius 5-20 μm, the visible albedo is quite high (90-95%) and nearly independent of wavelength. As the grain size increases, the snow albedo develops a peak at $\lambda \approx 0.5$ μm. For $r=2000$ μm the calculated albedo is as low as 35%. For a given grain size, the visible albedo of CO₂ snow is lower than of H₂O snow (Figure 4). This is because m_{jm} for H₂O ice is extremely small in the visible ($m_{\text{jm}} < 10^{-8}$), whereas CO₂ ice is considerably more absorptive ($m_{\text{jm}} \sim 10^{-6}$). (However, because of the possible influence of absorptive impurities in the unpurified commercial dry ice used to measure m_{jm} in the visible, these computed albedos for CO₂ snow may be too low.) By contrast, in the near-infrared the albedo is higher for CO₂ snow than for water snow because CO₂ ice is less absorptive than H₂O ice.

The albedo dips dramatically in the near-infrared absorption bands of CO₂ at 1.4-, 2.0-, and 2.7-μm wavelength. Comparison with Kieffer's [1968, 1970] laboratory reflectance spectra of CO₂ frosts between 0.8 and 3.2 μm shows overall agreement, for example that "the 2.7-μm band is saturated for frosts of textural scale greater than about 50 μm (i.e., $r=25$ μm) and has a minimum reflectance of 1%" [Kieffer, 1970, p. 503]; also that increase in grain size progressively deepens these absorption features.

But there are also disagreements with Kieffer's experimental results. Our 1.4-μm absorption feature is much stronger than his, probably because it is very narrow and was not resolved in the experiment. The three lines near 2 μm are merged into a single absorption feature in his spectrum. However, the 3-μm absorption feature is narrower in his observed spectrum than in our calculation. Since H₂O absorbs strongly at 3 μm, this could possibly be due to water ice contamination in the samples which Dittion and Kieffer [1979] used to obtain m_{jm} so that our calculation is contaminated by water, if Kieffer's frost spectra were measured on more carefully purified CO₂.

The reflectance spectrum of CO₂ frost has been extended into the ultraviolet by Wagner et al. [1987, Figure 16]. The reflectance remains high, increasing slightly as wavelength decreases from 400 to 300 nm (i.e., opposite to the trend in Figure 5a), then drops sharply to near zero at 220 nm.

A complication that we do not investigate in this paper is the possible increase of grain size with depth, which is common in terrestrial snow. This can affect the albedo differently at different wavelengths, because light penetrates more deeply into the snowpack in spectral regions of weak absorption and the albedo at those wavelengths is affected by the larger subsurface grains (T. C. Grenfell et al., manuscript in preparation, 1990).

Emissivity of Water Snow

In contrast to the albedo, which varies considerably with snow grain size and wavelength, the emissivity of water snow (Figure 6) is close to 99% for all grain sizes throughout the thermal infrared. This is because the absorption coefficient of H₂O ice is large enough ($m_{\text{jm}} \cdot x > 1$) that essentially all the light at these wavelengths which enters a snow grain is absorbed in the grain, but small enough ($m_{\text{jm}} \ll 1$) that external reflection at the surface of the grain is still small. The spectrally averaged emissivity $\bar{\epsilon}$ is given on each of the curves. Note that the scale of emissivity on Figure 6 runs only from 0.93 to 1.00, in contrast to the figures below for CO₂ snow.

Emissivity of CO₂ Snow

The emissivity of CO₂ snow (Figure 7), by contrast to that of water snow, should depend strongly on grain size, because $m_{\text{jm}} \cdot x \ll 1$ for all realistic grain sizes (i.e., small enough to give a high visible albedo) except in the 15-μm band. The model predicts emissivities in the IRTM surface-sensing channels which vary from less than 10% for $r=5$ μm to over 90% for $r=2000$ μm. The calculated emissivity is for viewing angle $\theta_{\text{out}}=60^\circ$, but this is also approximately the same as the hemispherically averaged emissivity. The most reliable parts of the curves are the region 6.5-8.6 μm, where m_{jm} is based on the accurate transmission measurements of Gaizauskas [1955] (reviewed by Warren [1986]). The curves are dashed in regions where m_{jm} is uncertain by more than a factor of 10, to indicate that the emissivity is also highly uncertain.

This low emissivity calculated for CO₂ snow is unusual for planetary surfaces, most of which have emissivity above 0.9 in the thermal infrared. The low emissivity is due to the small interband absorption coefficient. The spectrum of CO₂ ice is characterized by intense narrow absorption lines, which contrasts with that of other ices. Fink and Sill [1982, Figure 4] illustrated this, noting the contrast to the much smoother absorption spectrum of H₂O ice and attributing

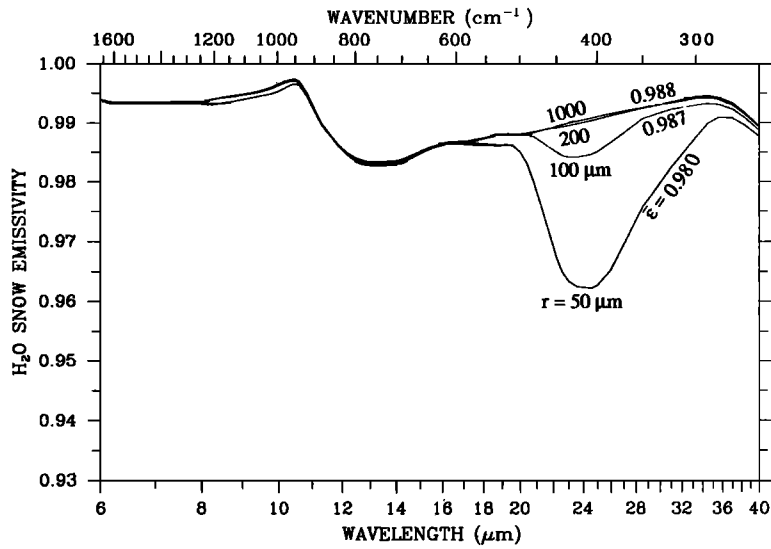


Fig. 6. Hemispherically averaged emissivity of water snow as a function of wavelength, calculated for various snow grain sizes. (From Figure 1a of Dozier and Warren [1982], but using revised values of optical constants of ice from Warren [1984].) Spectrally averaged emissivity $\bar{\epsilon}$ is also given.

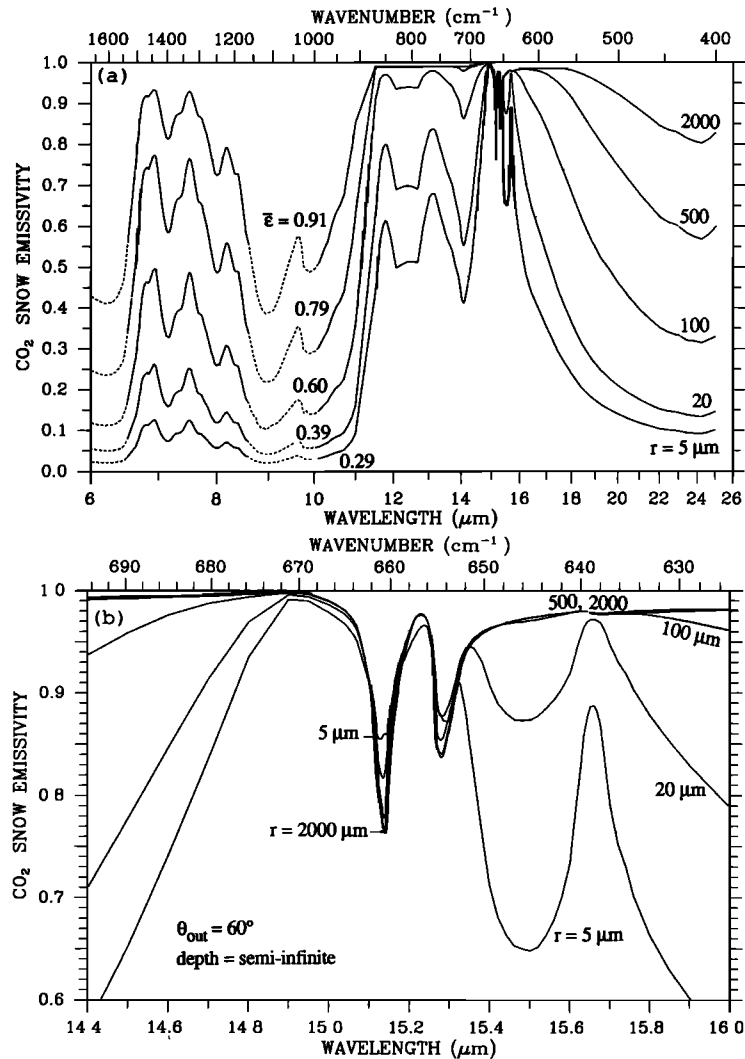


Fig. 7. Spectral emissivity of CO₂ snow calculated for various snow grain sizes, for viewing angle $\theta_{out}=60^\circ$ (approximately the same as the hemispherically averaged emissivity). Dashed curves are drawn for spectral regions where the imaginary refractive index is uncertain by more than a factor of 10. The $\bar{\epsilon}$ is an average emissivity for only about half the longwave spectrum (equation (2)).

the difference to the lack of hydrogen bonding in CO₂ ice: weaker interactions between molecules allow longer lifetimes for excited states and thus narrower absorption lines.

Because the emissivity varies greatly with wavelength and because the spectral distribution of incident longwave radiation differs from that emitted by the surface, surface energy budget calculations should ideally divide the longwave spectrum into several bands. Broadband models, which do not do this, require a spectrally averaged emissivity, but we cannot compute it because we have m_{im} values only for $\lambda < 25 \mu\text{m}$, representing only about half of the integral of the Planck function $B(\lambda, T)$ for $T = 148 \text{ K}$, a representative polar cap temperature. The $\bar{\epsilon}$ displayed on the graphs is therefore an average for only about half the longwave spectrum:

$$\bar{\epsilon} = \int B(\lambda, T) \epsilon(\lambda) d\lambda / \int B(\lambda, T) d\lambda \quad (2)$$

where the limits of integration are 6 and 25 μm .

Ignoring other possibilities to be discussed below, the observed poleward decrease in the 20- μm channel brightness temperature T_{20} in winter [Kieffer et al., 1977] suggests that snow grain size decreases toward the pole. This would be reasonable if the snow was still being deposited at the pole but not at the edge, so that the surface snow at the cap edge had more time to undergo metamorphism, which normally leads to larger grains. However, most models predict CO₂ deposition at both the center and the edge during the winter season.

Without taking into account the detailed spectral response of the channels, Figure 7 suggests that for a given grain size, the emissivity at 20 and 7 μm should be larger than that at 9 and 11 μm . This does not agree with the Viking IRTM data [Kieffer, 1979], which showed $T_9 > T_{11} > T_{20}$ over the south polar cap. However, in order to make detailed comparisons with Viking data it will be necessary to obtain channel emissivities by multiplying $\epsilon(\lambda)$ by the spectral response function $W(\lambda)$ of the channel [Kieffer et al., 1977, Figure 1] and the Planck function $B(\lambda, T)$:

$$\epsilon_{\text{channel}} = \int \epsilon(\lambda) W(\lambda) B(\lambda, T) d\lambda / \int W(\lambda) B(\lambda, T) d\lambda$$

Because our calculations are based on highly uncertain values of $m_{im}(\lambda)$, we think it premature to do such detailed comparisons until $m_{im}(\lambda)$ is remeasured throughout this wavelength region.

Figure 7b shows reflection peaks at $\lambda = 15.13$ and 15.28 μm . This is due to external reflection from snow grains because of the large m_{im} at these wavelengths [Warren, 1986, Figure 15f].

Dependence of Emissivity on Snow Density

As discussed by Dozier and Warren [1982], interparticle interference ("near-field effects") may cause the emissivity to depend on snow density. The effect is apparently insignificant if $d \gg \lambda$, where d is the center-to-center separation of the particles. It becomes more significant with increasing wavelength in the thermal infrared. We ignore near-field effects elsewhere in the paper, but here we estimate their possible magnitude, which should be kept in mind when examining the other figures.

Dozier and Warren used the method of Gate [1973] to estimate the dependence of emissivity on density for water snow. Mie theory uses the refractive index of the particle relative to that of the medium. Gate's adjustment, as we apply it to CO₂ snow, is to take the real refractive index of

the medium not that of air (or vacuum) but rather of a mixture of air and CO₂ ice whose volume fractions are those within a shell one wavelength thick surrounding the particle [Warren, 1982, Figure 4]. The details are given by Dozier and Warren [1982].

Figure 8 shows the calculated emissivity of CO₂ snow incorporating this near-field adjustment. The effect is substantial for small grains at high density, but in snow the highest densities are usually associated with the largest grains. We do not know the range of densities for Martian snow, but Figure 8 raises the possibility that variations of emissivity, especially in the 20- μm channel, could be due to variations in density. In summary, incorporation of near-field effects raises the longwave emissivity but does not decrease the solar albedo.

Effect of Solar Zenith Angle or Infrared Emission Angle

The range of solar zenith angles experienced over the southern polar cap is about 50°-90°, as can be seen in Figure 9, which is based on the observed springtime recession of the cap edge given in Figure 18 of James et al. [1979].

Figures 10a and 10b show that the albedo (for $r = 100 \mu\text{m}$) increases at all wavelengths as the solar zenith angle increases from 0° to 80°. In the albedo calculation the zenith angle θ_0 enters only as its cosine μ_0 , so the albedo is more sensitive to θ_0 at low sun than at high sun. Kieffer's [1968] observations support this: he found reflectance to vary insignificantly for incidence (zenith) angles between 0° and 45°.

The reason that the albedo is higher for low sun is that a photon on average undergoes its first scattering event closer to the surface if it enters the snow at a grazing angle. If the scattering event sends it an upward direction, its chance of escaping the snowpack without being absorbed is greater than it would be if it were scattered from deeper in the pack.

These calculations are for a flat surface; because of surface roughness on a natural snow surface, the effective zenith angle will rarely be as large as 80°. Also, scattering of the solar beam by the atmosphere will change the effective zenith angle, bringing it toward the effective zenith angle of diffuse radiation which is about 50° (section 5d of WWI).

The observation by Kieffer [1979] that the early spring albedos were highest near the cap edge is opposite to that expected from the zenith angle dependence. However, the Lambertian reflectance assumption used to convert satellite-measured radiances into albedos would have been inaccurate at the very large solar zenith angles occurring near the pole at this season. The bidirectional reflectance of water snow becomes more anisotropic at low sun [Warren, 1982, Figure 14], and that of CO₂ snow probably does as well [Paige and Ingersoll, 1985, Figure 4]. Furthermore, at large zenith angles the bidirectional reflectance of the Martian atmosphere may also contribute significantly to the reflected radiation, so that it is not just the surface that is being seen.

Figures 10c and 10d show that the emissivity into the overhead direction is larger than for limb exitance. This will influence the brightness temperatures seen from satellites, as discussed by Dozier and Warren [1982]. The dependence of ϵ on the look angle θ_{out} is the likely explanation for the observation by Kieffer et al. [1977] that the lowest brightness temperatures generally appeared 2° of latitude beyond the pole, whatever azimuth the pole was viewed from.

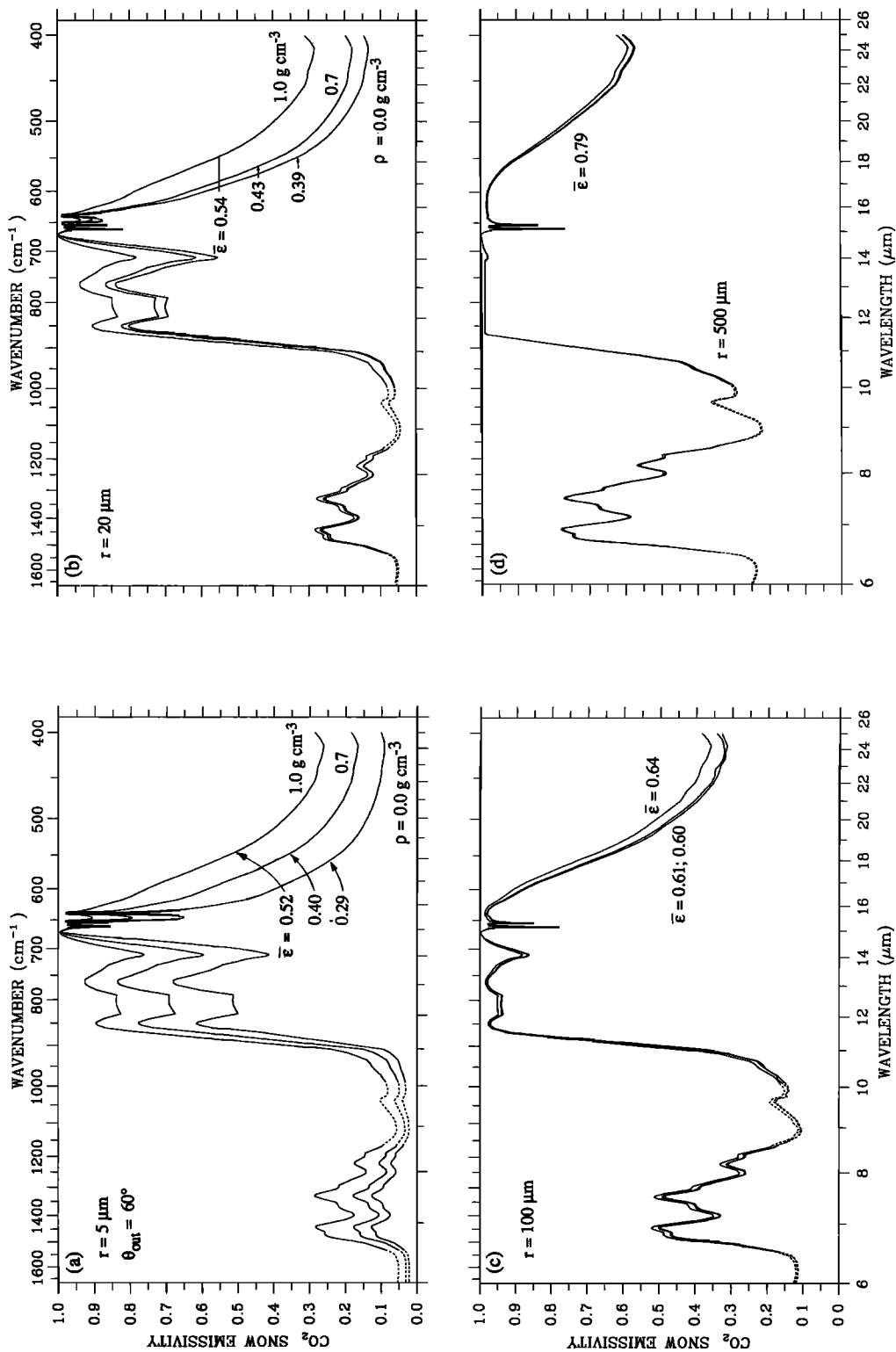


Fig. 8. Near field effect on spectral emissivity of CO₂ snow. Grain radii r from 5 to 500 μm are shown, for snow densities ρ from 0.0 to 1.0 g cm^{-3} . Density $\rho=0$ corresponds to the absence of any near-field effect.

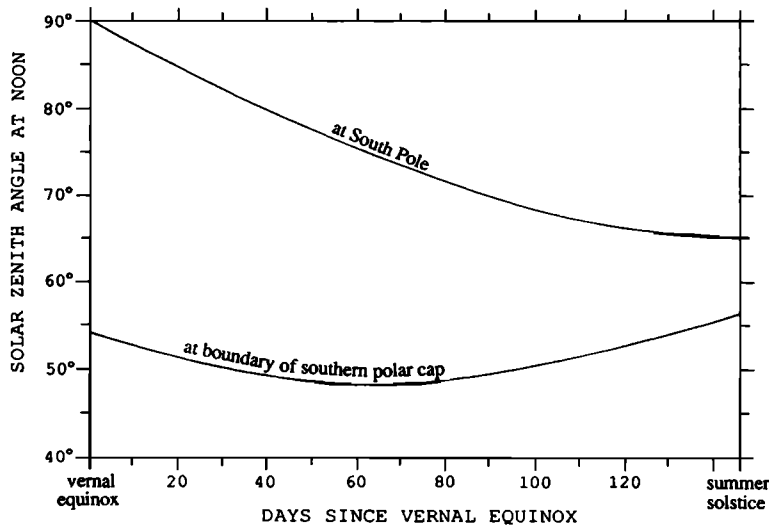


Fig. 9. Noontime solar zenith angle during spring at the edge of the Martian south polar cap and at the south pole. (Polar cap edge data are from Figure 18 of James et al. [1979].)

For the calculations below we use a standard solar zenith angle (or infrared viewing angle) of 60°. This is a typical solar zenith angle for noon at a latitude about 10° poleward of the south polar cap edge at any time during spring.

Effect of Finite Snow Depth

The results shown so far are all for semi-infinite snow. Here we determine how thick a snowpack must be to be effectively semi-infinite. Figure 11 shows albedo and emissivity for various depths of CO₂ snow, where depth is expressed as mass per unit area.

To compute Figure 11, we needed the spectral albedo of the underlying surface. To estimate this we made use of the relative reflectance spectra of Martian soil shown in Figure 3 of Singer et al. [1979] for 0.3 to 2.5 μm wavelength. We scaled these spectra to obtain an average shortwave albedo of 0.25, typical of Martian soil. To extend these results to shorter and longer wavelengths, we assumed that the value at 0.3 μm applies also to the region 0.2-0.3 μm , and that the value at 2.5 μm applies also to the region 2.5-6 μm . For $\lambda > 6 \mu\text{m}$ the soil is assumed to be a blackbody emitter. The assumed spectrum of the underlying surface is shown as the dashed line in Figures 11a and 11b. It is unlikely to be correct for 2.5-6.0 μm , but the results in Figure 11 are insensitive to this choice (as opposed to a black underlying surface) if the snow thickness is greater than 0.2 g cm^{-2} .

Figure 11 shows that the semi-infinite limit is reached already at 0.1 g cm^{-2} in the absorption bands and at 0.5 g cm^{-2} in most parts of the thermal infrared. In the solar spectrum the albedo for 0.5 g cm^{-2} of snow is within 2% of the semi-infinite limit. The semi-infinite limit requires greater depths for larger grain sizes (Figure 13 of WWII).

In the visible, the depth of an effectively semi-infinite CO₂ snowpack is about a factor of 4 smaller than that of a water snowpack (Figure 13 of WWII), because of the smaller visible absorption coefficient of water ice.

Observations of atmospheric pressure [Hess et al., 1979] indicate a mean thickness of 36 g cm^{-2} for the southern polar cap at its maximum extent. This is a factor of about 50 larger than needed to be effectively semi-infinite.

However, a model of growth and decay of the ice cap [Davies et al., 1977, Figure 6] indicates that during growth in the winter, snow at the edge of the cap may take about 20 days to reach a depth of 1 g cm^{-2} . Furthermore, the snow may be blown by the wind to leave bare patches or regions of thin snow; James et al. [1979] thought this to be responsible for the variability of observed visible snow albedo across the polar cap. Therefore, even though the finite depth effect is apparent only for depths less than 1 g cm^{-2} , this condition may apply over large areas of the Martian high latitudes.

Effect of Dust Content

Except in Antarctica, the observed visible albedo of water snow on Earth is often not as high as that predicted by the model for pure snow, although near-infrared albedos agree rather well. Warren and Wiscombe [1980] (hereinafter referred to as WWII) proposed that absorptive impurities in the snow were responsible for this discrepancy. Visible snow albedo can be reduced several percent by the addition of 10 parts per million (ppm) by mass of desert dust or 0.1 ppm of carbon soot, but these trace impurities have no effect on snow albedo or emissivity for $\lambda > 1 \mu\text{m}$ where ice itself absorbs significantly. The model calculations were supported by field measurements of albedo and laboratory analysis of soot by Grenfell et al. [1981], as discussed by Warren [1982].

Clay mineral dust is likely to be important in affecting the albedo of both H₂O snow and CO₂ snow on Mars. Because the Martian atmosphere is so dusty, some of the dust will reach the snow surface. Pollack et al. thought it likely that CO₂ snow nucleates on dust particles. Toon et al. [1980] estimated the volume mixing ratio of dust in CO₂ snow to be 10⁻³ in the north polar cap and 10⁻⁴ in the south and showed that it should affect the snow albedo.

To calculate the albedo or emissivity of snow containing dust, we follow the methods used by WWII. Mie calculations are done separately for the dust particles and the ice particles and then averaged using the respective cross-sectional areas per unit volume as weighting factors. The calculation assumes that the dust particles are separate from the ice particles. If the dust particles are instead located

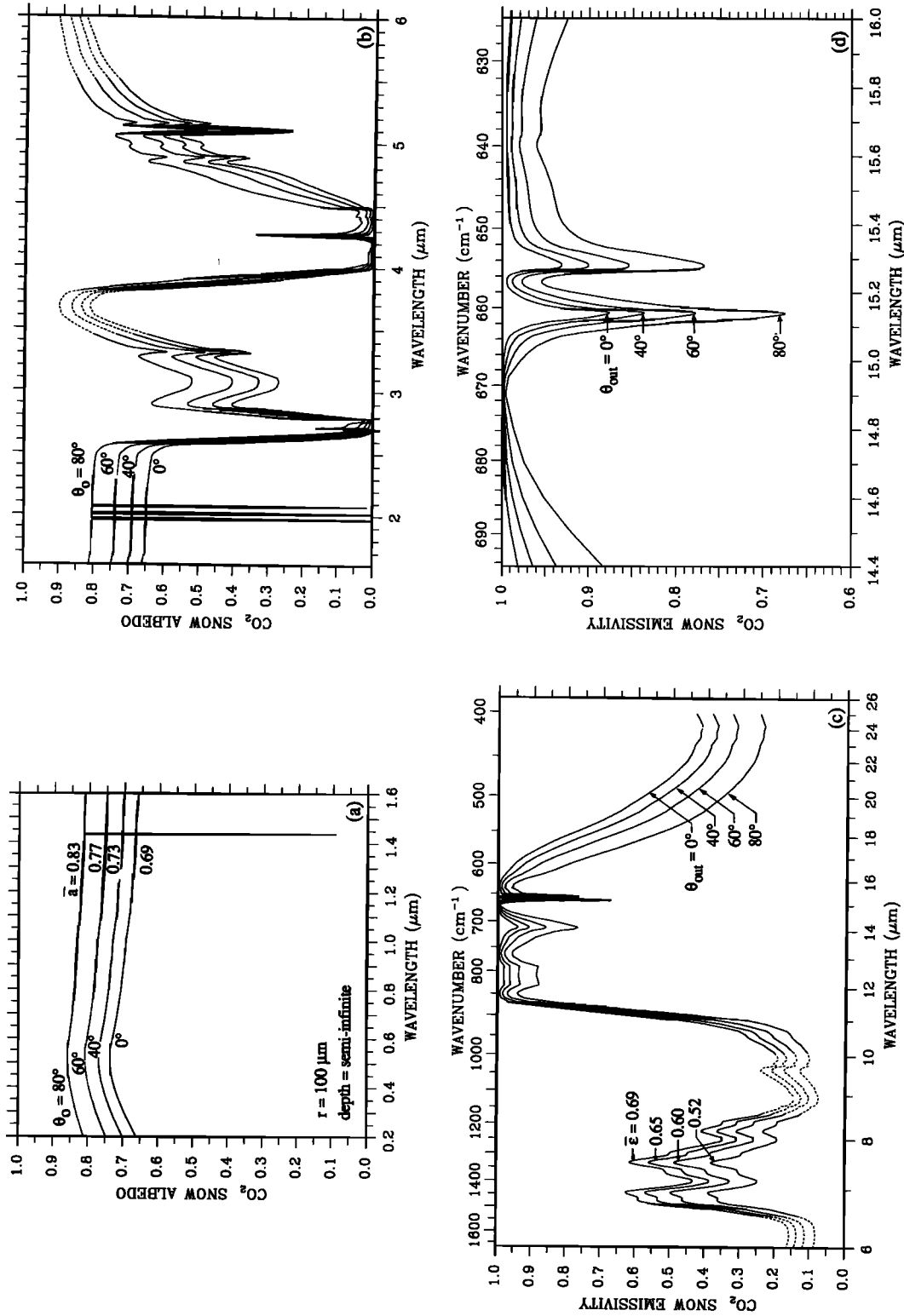


Fig. 10. Effect of solar zenith angle or infrared viewing angle on spectral albedo and emissivity of a semi-infinite CO₂ snowpack ($r=100 \mu\text{m}$).

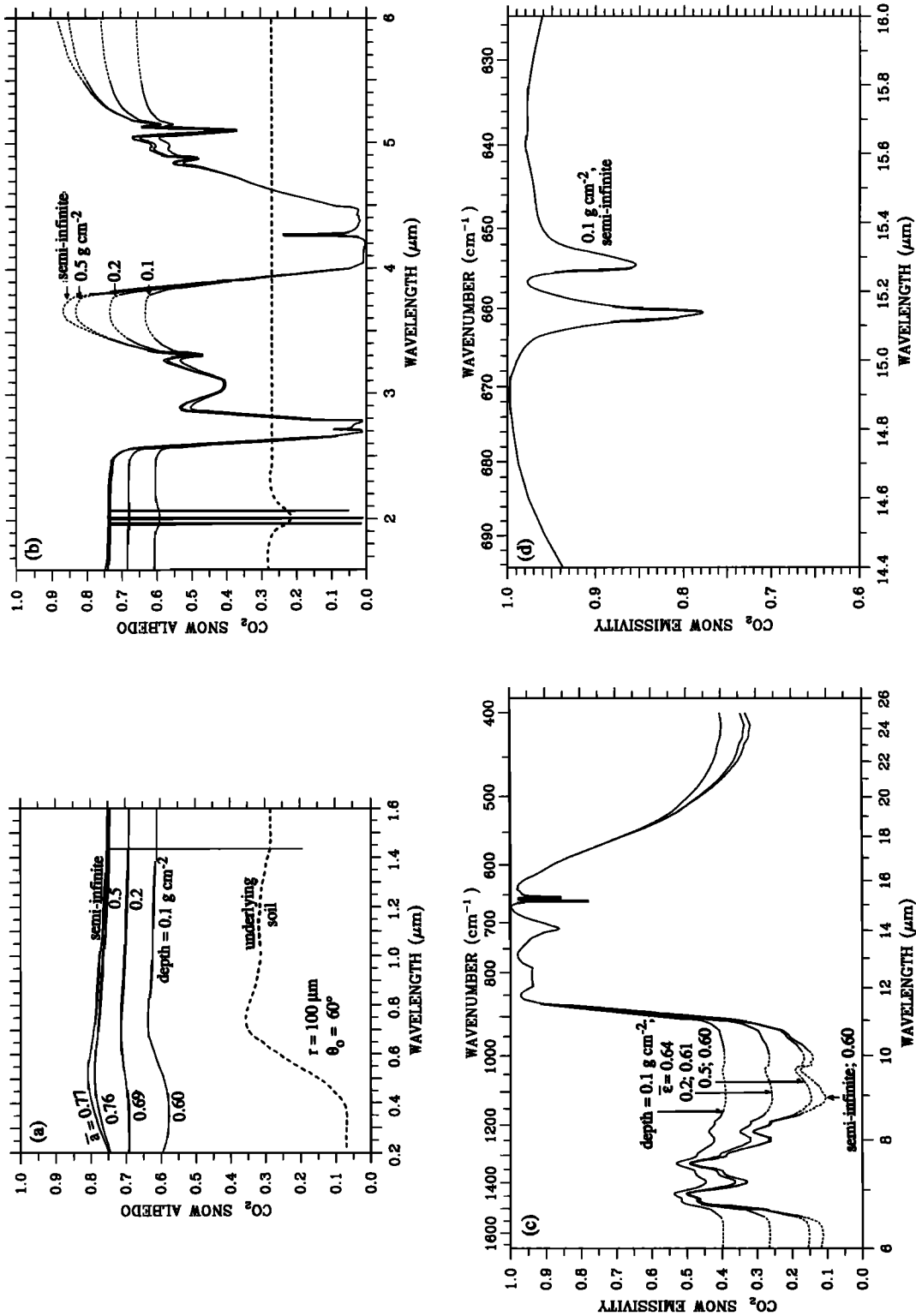


Fig. 11. Direct-beam spectral albedo and directional emissivity ($\theta_0=60^\circ$) of a thin snowpack, for a variety of snow depths, for CO₂ snow ($r=100 \mu\text{m}$) over a surface of dark Martian soil (underlying albedo shown as a dashed line). The soil is assumed black for $\lambda > 6 \mu\text{m}$.

inside the ice particles (whether in H₂O ice or CO₂ ice), they may be more effective at absorbing radiation, such that the effects we attribute to a particular concentration of dust may actually result from only half that concentration [Bohren and Huffman, 1983, p. 446; Chylek et al., 1983; Bohren, 1986].

Pollack et al. [1979] fitted the angular variation of Martian sky brightness (observed by the Viking lander) best by using an optically effective $\bar{r}_{\text{dust}}=2.5 \mu\text{m}$; we use this radius for our calculations on the presumption that it is also representative of dust in snow. We assume the dust has a density of 2.6 g cm^{-3} , typical of clay minerals.

The albedo of pure water snow is rather flat in the visible. Figure 12 shows that adding dust reduces the albedo and gives it a stronger spectral dependence, with higher albedo for red light than for blue. The dust has no effect on albedo or emissivity beyond $1.4 \mu\text{m}$ wavelength.

Figure 13 shows that dust also reduces the albedo of CO₂ snow (except in the 2.7- and 4- μm bands), but because

CO₂ ice is more absorptive than H₂O ice about 5 times as much dust is required to reduce the albedo by a comparable amount in CO₂ snow.

Martian surface albedos for the polar cap were inferred by James et al. [1979] at $\lambda = 0.59 \mu\text{m}$ (*a_{red}*) and $\lambda = 0.44 \mu\text{m}$ (*a_{blue}*). The ratio *a_{red}*/*a_{blue}* in Figure 13a is smaller than was observed, suggesting that $m_{\text{im}}(\lambda)$ for Martian dust may actually depend more steeply on wavelength than we have assumed, in the spectral region 0.3-0.7 μm .

The surface albedo inferred by James et al. depended on the optical depth τ they assumed for the atmosphere. For the residual south cap the surface albedos (*a_{red}*, *a_{blue}*) were (0.93, 0.73) assuming $\tau=0.1$, or (0.65, 0.52) assuming $\tau=0$. The former values are not consistent with any of our snow albedo calculations, dusty or clean, CO₂ or H₂O, perhaps suggesting that the optical depth was less than 0.1.

Earlier Earth-based measurements of the south polar cap with four colored filters [Lumme, 1976] are in qualitative agreement with James et al., also suggesting the pres-

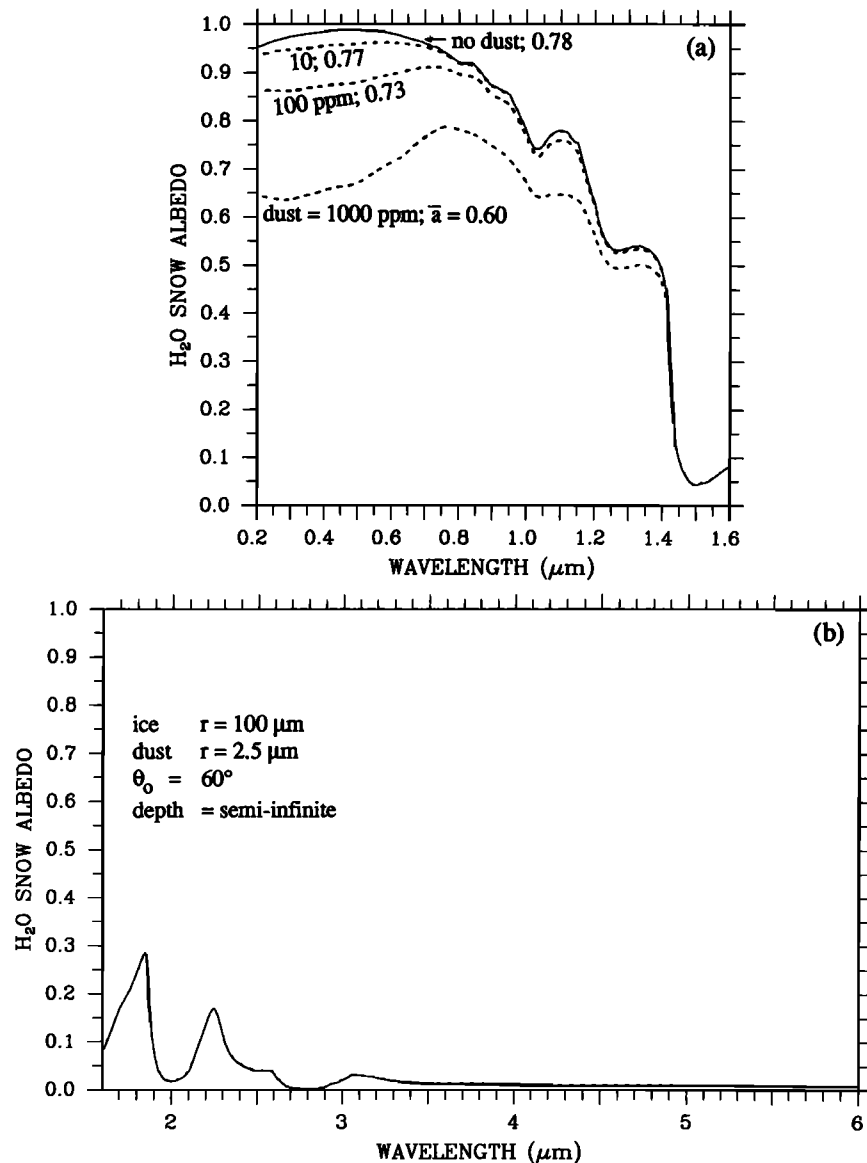


Fig. 12. Effect of Martian dust ($r=2.5 \mu\text{m}$) on calculated albedo of water snow ($r=100 \mu\text{m}$), as a function of wavelength. Dust concentrations are given as mass fractions. (Similar to Figure 5a of Warren and Wiscombe [1980] but using Martian dust instead of Saharan dust and using revised optical constants of ice from Warren [1984].)

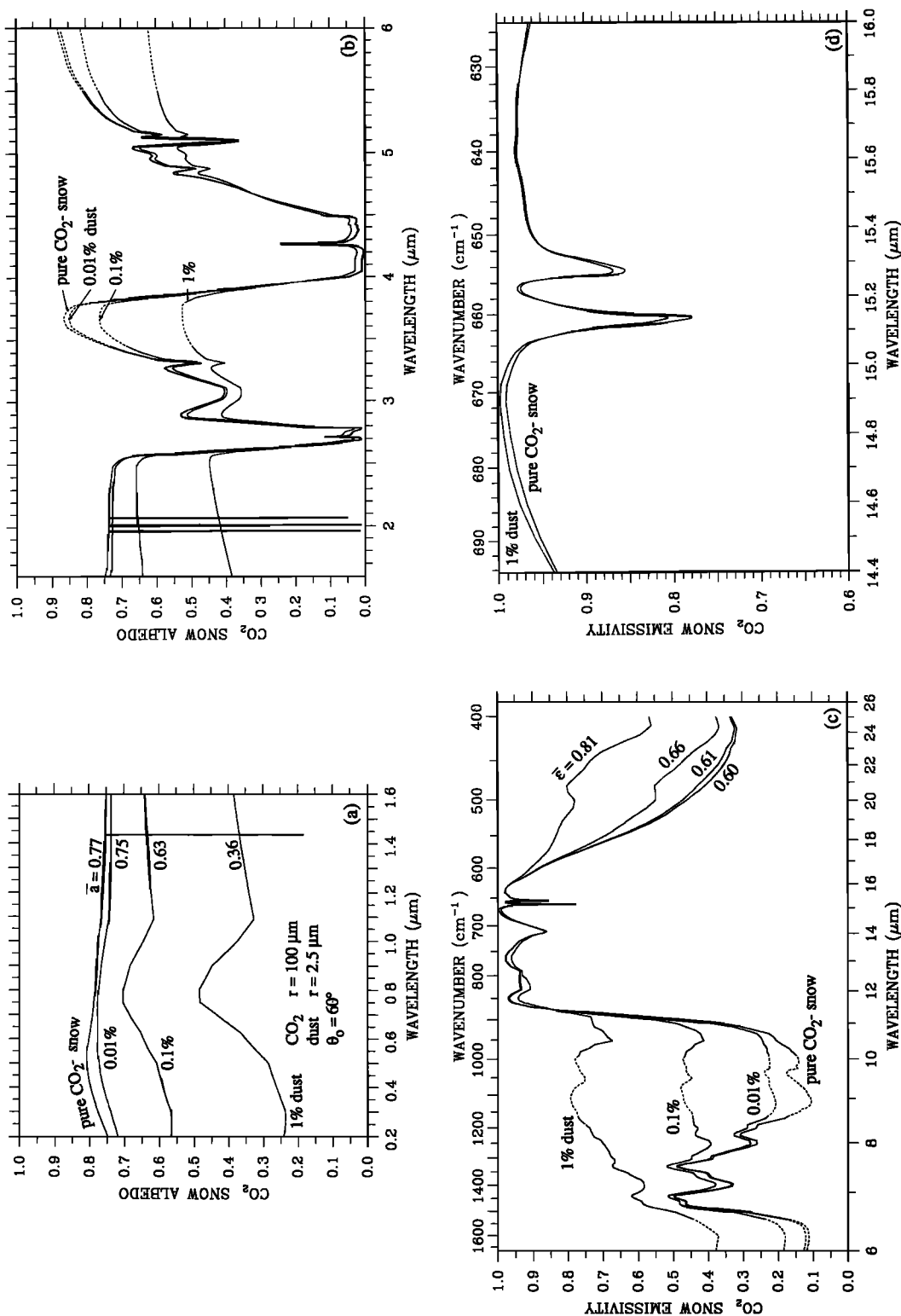


Fig. 13. Effect of Martian dust ($r=2.5 \mu\text{m}$) on spectral albedo and emissivity of CO₂ snow ($r=100 \mu\text{m}$). Dust concentrations are given as mass fractions. Dust optical constants are for Martian dust as described in the text.

ence of dust. Lumme had to deconvolute the raw data because his field of view extended beyond the polar cap. The derived albedos were 0.53 at $\lambda=435$ nm, 0.60 at 550 nm, and 0.68 at 580 and 620 nm.

Dust also causes an increase in the longwave emissivity of CO₂ snow (Figure 13c). However, the effect of dust is only a few percent for the small dust amount (0.01%) suggested by Toon et al. [1980] for the south cap. It is only when the dust content reaches 0.1% that the effect becomes substantial. The dust content may decrease poleward, as the snow becomes more remote from sources of dust, but there are also bare areas even within the cap area which could be sources of dust. Adding dust should raise the emissivity more in spectral regions where the emissivity is low, so it should reduce the brightness-temperature differences among channels. Kieffer's [1979] observation that these brightness-temperature differences increased after a dust storm suggests that the infrared spectrum of Martian dust may be different from what we assumed.

Kieffer's [1979, Figure 4] observation that the planetary albedo of the south pole increased after the first global dust storm is puzzling. Adding dust to snow, or to the atmosphere above the snow, would cause the albedo to decrease unless the dust caused clouds to form. However, after the second global dust storm the planetary albedo decreased at the south pole as expected [Kieffer 1979, Figure 11].

Effect of Water Content

Another contaminant in CO₂ snow which can affect the albedo and emissivity is water. The total precipitable water over Mars' Antarctic varies from <1 μm in winter to 10-15 μm in summer [Davies and Wainio, 1981]. (By comparison, the precipitable water over the antarctic plateau on Earth varies from 20 μm in winter (when most of the snow accumulation occurs) to 300 μm in summer [Kuhn, 1972, Table 13]).

Some of the features in Earth-based near-infrared spectra of the north seasonal polar cap were attributed to water ice by Clark and McCord [1982] (corrected by Jakosky [1983]). Water is not so obvious in the south seasonal cap: Larson and Fink [1972] were unable to find water ice features in Earth-based near-infrared spectra during southern spring, but Pimental et al. [1974] did detect water ice in the Mariner spectra.

Kieffer [1968, 1970] investigated the effect of water content in the laboratory for 0.8-3.2 μm wavelength and H₂O mixing ratios from 0.8% to 23%. At the lowest mixing ratios only the 3.1- μm band of H₂O was noticeable in the reflectance spectrum, but with 10% water the spectrum was dominated by water, and CO₂ could only be identified by its absorption at 2.7 μm . In most of the near-infrared, H₂O is more absorptive than CO₂, so, as Kieffer [1970, p. 501] noted, "...the addition of small amounts of H₂O made appreciable changes in the CO₂ spectra, but not vice versa."

The results of mixing water ice into CO₂ snow are shown in Figure 14, where we have arbitrarily assumed that the water is present as separate ice particles of size $r=10$ μm , such as cloud particles on which the CO₂ snow might have nucleated. The presence of water ice raises the albedo slightly in the visible (for more than 1% H₂O) but reduces it elsewhere in the solar spectrum. This causes a curious behavior in the spectrally averaged albedo: as water content is increased from zero to 10% the first effect is to lower the near-infrared albedo, reducing \bar{a} , but as the water content continues to increase beyond 10% the near-infrared

saturates while the visible albedo rises, increasing \bar{a} . However, these changes in \bar{a} are at most a few percent.

The addition of water dramatically raises the emissivity of CO₂ snow over essentially the entire thermal-infrared spectrum. The observed decrease of 20- μm emissivity toward the south pole could thus be the result of a drier atmosphere leading to less contamination of the snow with water ice. However, more than 0.01% H₂O is necessary to have an appreciable effect on the longwave emissivity, if it is uniformly mixed with CO₂. This is the mixing ratio of H₂O in the average Martian atmosphere and is the expected mixing ratio of H₂O in deposited CO₂ snow [Kieffer, 1990].

However, the water ice is unlikely to be uniformly mixed. In springtime the H₂O (and dust) should accumulate at the surface of the snowpack as a "lag deposit" [Jakosky, 1985], where they can dominate the emissivity. In summer over the residual south polar cap, water vapor is likely to deposit onto the surface as a fine-grained frost, reaching a thickness of 0.05-0.2 g cm⁻² [Jakosky and Haberle, 1990; Haberle and Jakosky, 1990]. Kieffer [1990] modeled the metamorphism of H₂O frost and predicted that the deposit should initially have grain radius $r<10$ μm , growing to 50-100 μm in a year.

Figures 15 and 16 show the effect of adding a thin surface layer of pure H₂O snow over a semi-infinite CO₂ snowpack. Figure 15 uses H₂O grain radius $r=100$ μm ; Figure 16 uses 10 μm . Figure 15 shows that the albedo drops slightly when the H₂O layer is added, because the small increase in visible albedo is more than compensated by the large decrease in near-infrared albedo. The change in average albedo is only a few percent, so the H₂O layer has little effect on the solar energy budget. Water is much more important for the longwave budget: the average emissivity is dramatically increased even for the thinnest surface layer (0.002 g cm⁻² H₂O).

The H₂O frost layer has quite different effects if it consists of 10- μm grains. Only 0.002 g cm⁻² H₂O is enough to almost completely hide the underlying CO₂ in the thermal infrared (Figure 16c), whereas 10 times as much H₂O was needed if the grain radius was 100 μm (Figure 15c). However, the asymptotic emissivity is 10% lower for the fine-grained frost. In the visible, the fine-grained frost raises the albedo sufficiently to overcome the near-infrared reduction, so it causes a few percent increase in \bar{a} .

If pure H₂O frost is deposited on the residual south polar cap in summer, the underlying surface is likely to contain a substantial amount of dust which became concentrated as the CO₂ sublimated. Figure 17 shows how the addition of a thin layer of H₂O frost causes the albedo to increase. This is the only situation in which the addition of small amounts of water ice can increase \bar{a} significantly. The increase is much larger for the fine-grained frost (Figure 17b) than for the coarse-grained frost (Figure 17a).

H₂O can also combine chemically with CO₂ to form a clathrate containing about 80% H₂O, but the spectrum of this clathrate is very similar to that of H₂O ice [Smythe, 1975], so this possible form of a CO₂-H₂O mixture is unlikely to complicate inferences about water content from spectral observations of the polar caps.

Effect of Surface Roughness on Albedo and Emissivity

All our calculations are for a flat CO₂ snow surface, i.e., a surface whose irregularities are of a scale smaller than the flux penetration depth of radiation. Surface roughness

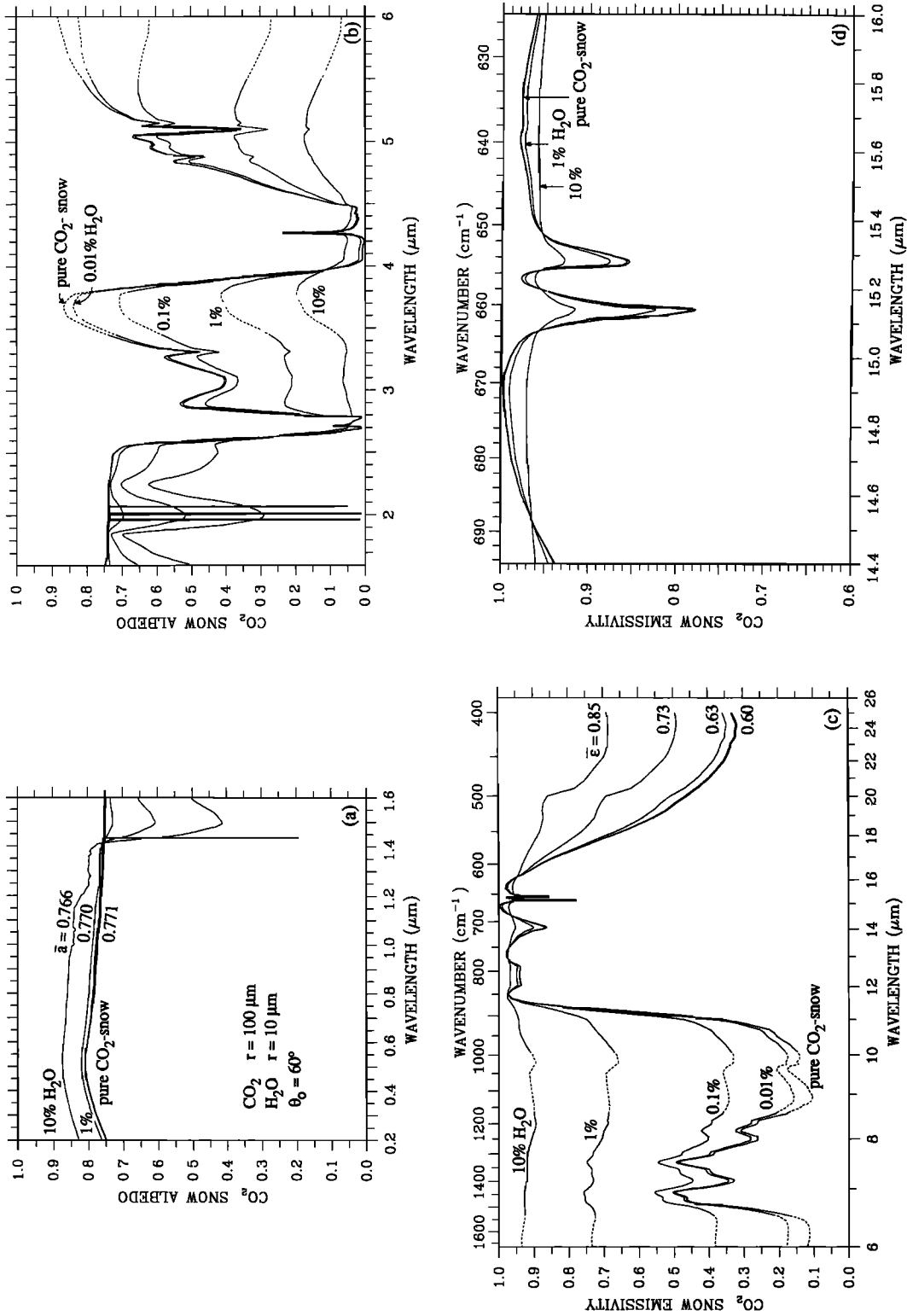


Fig. 14. Effect of water-ice contamination (r=10 μm) on spectral albedo and emissivity of CO₂ snow (r=100 μm). Water ice concentrations are given as mass fractions, assumed homogeneously mixed.

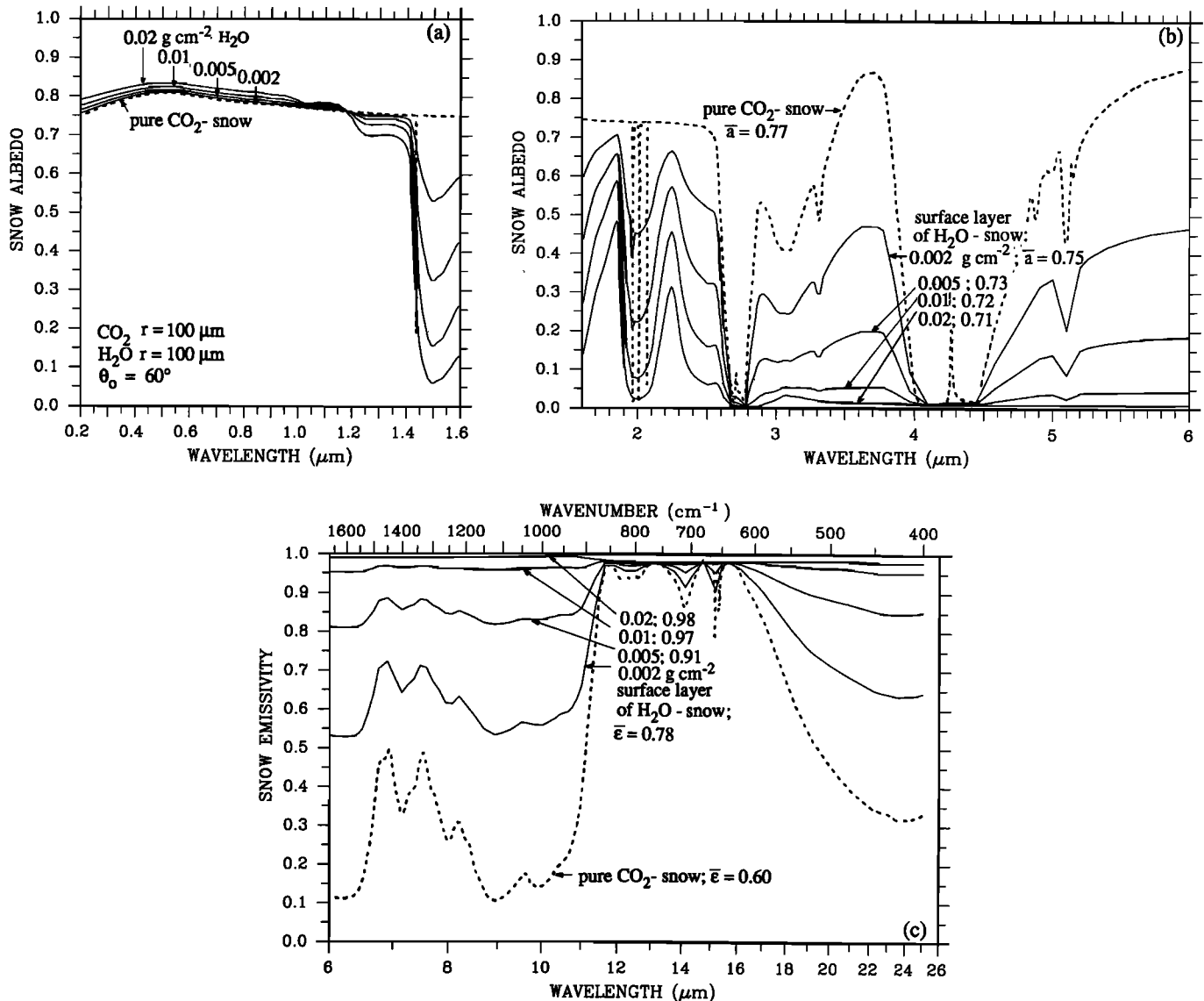


Fig. 15. Spectral albedo and emissivity of pure CO₂-snow (r=100 μm) covered by a layer of water snow (r=100 μm) of various thicknesses.

may exist on Martian snow as it does on terrestrial snow in the form of sastrugi, which are longitudinal dunes formed by wind erosion [Gow, 1965]; or penitents, which are vertical wedges formed by differential sublimation [Lliboutry, 1954; Rhodes et al., 1987]. Surface roughness generally causes a reduction of albedo and an increase of emissivity, relative to a flat surface, due to "trapping" of reflected photons [Warren, 1982]. It causes much greater changes to the bidirectional reflectance distribution function. Because there is insufficient information about the magnitude of surface roughness on Martian polar caps, we have not modeled these effects.

Sensitivity of Albedo and Emissivity to Uncertainty in Absorption Coefficient

The uncertainty in the absorption coefficient of CO₂ ice varies considerably with wavelength. Warren's [1986, p. 2672] summary stated: "The imaginary index is probably accurate to ±20% from 0.3 to 1.0 μm and from 6.6 to 8.6 μm. In the UV and in the strong bands the uncertainty of

both m_{im} and m_{re} is a factor of ~2. In the infrared, outside the strong bands, the uncertainty is a factor of ~5 except . . . near 3.6, 6, and 9 μm [dashed lines in our graphs], where the uncertainty is more than a factor of 10." The real index outside the strong bands is uncertain only to about ±0.05, so the albedo and emissivity are much more sensitive to errors in m_{im} than to errors in m_{re} . Figure 18 shows the albedo and emissivity for r=100 μm which results from multiplying or dividing m_{im} by 2 or 5 at all wavelengths. (This was not done in the bands at 4.3 and 15 μm because m_{im} is unlikely to be much in error there and because altering m_{im} in the bands would affect m_{re} as well.) A factor of 2 uncertainty in m_{im} causes ±10% uncertainty in the calculated albedo and emissivity. A detailed interpretation of Martian radiation data would thus benefit from more accurate laboratory measurements of the complex refractive index of solid CO₂.

Summary

A snow albedo model previously developed for terrestrial snow is extended to the case of CO₂ snow. Pure CO₂

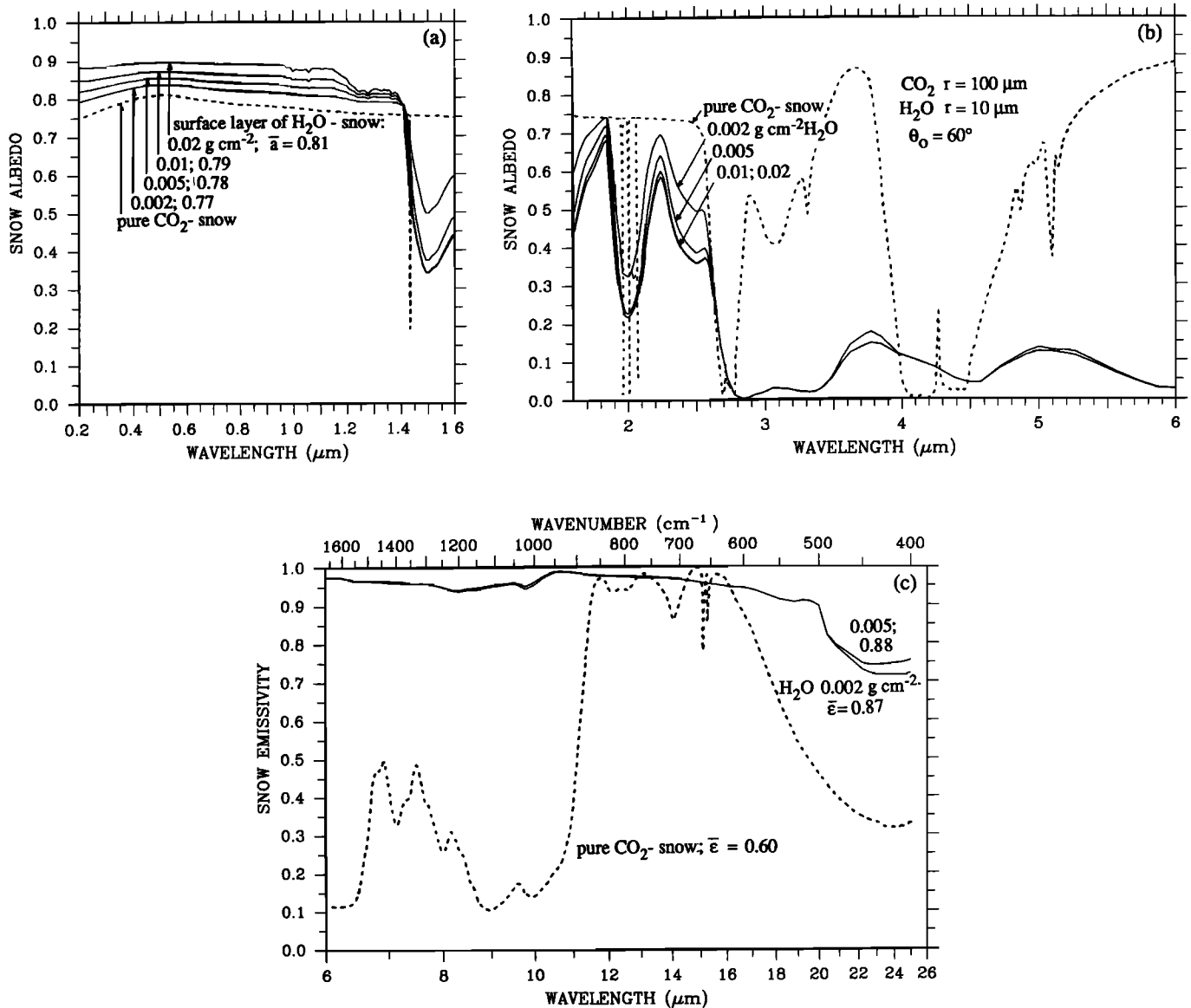


Fig. 16. Same as Figure 15 but with $r=10 \mu\text{m}$ for water snow.

snow is calculated to have high albedo at visible wavelengths (75-80% for grain radius $100 \mu\text{m}$) but not as high as that of water snow (albedo > 95%). Albedos measured to be significantly lower than these values are not necessarily evidence of larger grains; they could be due to thin snow, or dirty snow, or subpixel dirty patches within the polar cap. The near-infrared albedo of CO₂ snow is higher than that of water snow.

At any given wavelength, the primary variable controlling albedo and emissivity is the snow grain size, with albedo decreasing and emissivity increasing as grain size increases, which probably happens as the snow ages. Of secondary importance is the solar zenith angle (or infrared emission angle), albedo increasing with zenith angle.

The average thickness of the winter snow cover on Mars is probably only about 1 m, but this is effectively semi-infinite: only about 0.5 g cm^{-2} of CO₂ snow is needed to hide the underlying soil so that it does not affect the albedo.

Observations (both from Earth and from Viking orbiters) that red albedo is much higher than blue albedo in

the Martian south polar cap indicates that the snow (or the atmosphere) is contaminated with red dust.

The absorption coefficient of CO₂ ice in the thermal infrared is 2-3 orders of magnitude smaller than that measured for H₂O ice, apparently due to the absence of hydrogen bonding in CO₂. Therefore, whereas water snow emissivity is very close to 100% for all grain sizes and emission angles, CO₂ snow emissivity is calculated to be much lower, varying substantially with wavelength, and quite sensitive to grain size and emission angle. Such low and variable emissivity is unusual for a planetary surface. The wavelength variations in emissivity are correlated with the spectral opacity of a CO₂ atmosphere. This means that energy budget calculations should be done in spectral detail.

Factors tending to increase emissivity are large grain size, small emission (viewing) angle, and large concentrations of dust or water. The poleward decrease of 20- μm brightness temperatures observed by Viking orbiters over the south polar cap in winter could thus be due to the expected changes in any of these four variables, to the extent that the surface is not hidden by clouds.

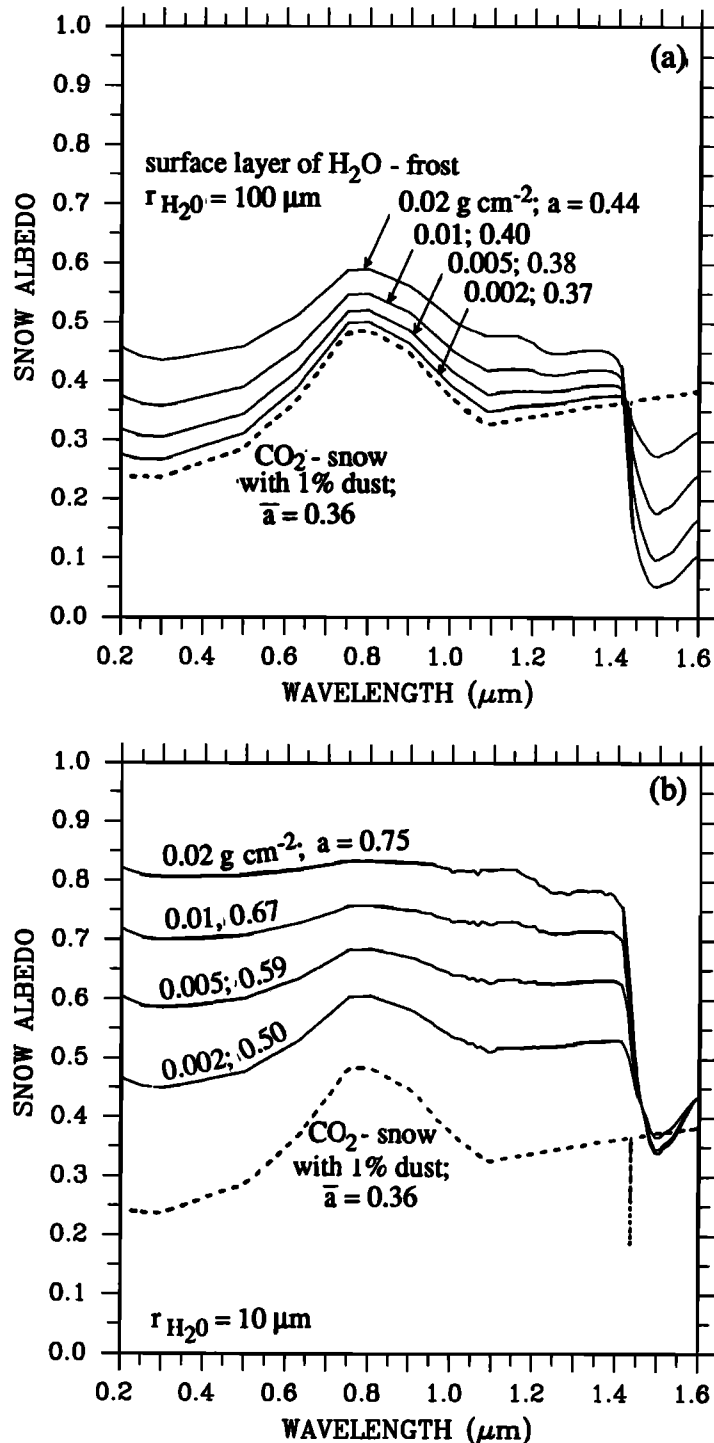


Fig. 17. Spectral albedo (at $\theta_0=60^\circ$) of dirty CO₂ snow ($r=100 \mu m$ for CO₂; $r=2.5 \mu m$ for dust), covered by a layer of water frost of various thicknesses. (a) Water frost grain radius $r=100 \mu m$. (b) $r=10 \mu m$.

Albedo is independent of snow density (for a given grain size), but the thermal emissivity, especially of fine-grained snow at longer wavelengths, increases with snow density. Thus variations in density could cause variations in brightness temperature in the 20-μm channel more than in the other IRTM channels on Viking.

Remote sensing of CO₂ grain size, H₂O content, and dust content may be possible because they have different effects in different spectral regions. Dust and H₂O both

cause emissivity to increase at 6 and 9 μm, but dust causes visible albedo to decrease whereas H₂O causes it to increase slightly. Emissivity at 7 μm is particularly sensitive to CO₂ grain size if the water content is not too large. However, the possible presence of dust, water ice, and CO₂ ice in the atmosphere will complicate the determination of surface properties. The design of a remote-sensing strategy awaits more accurate determination of the optical constants of CO₂.

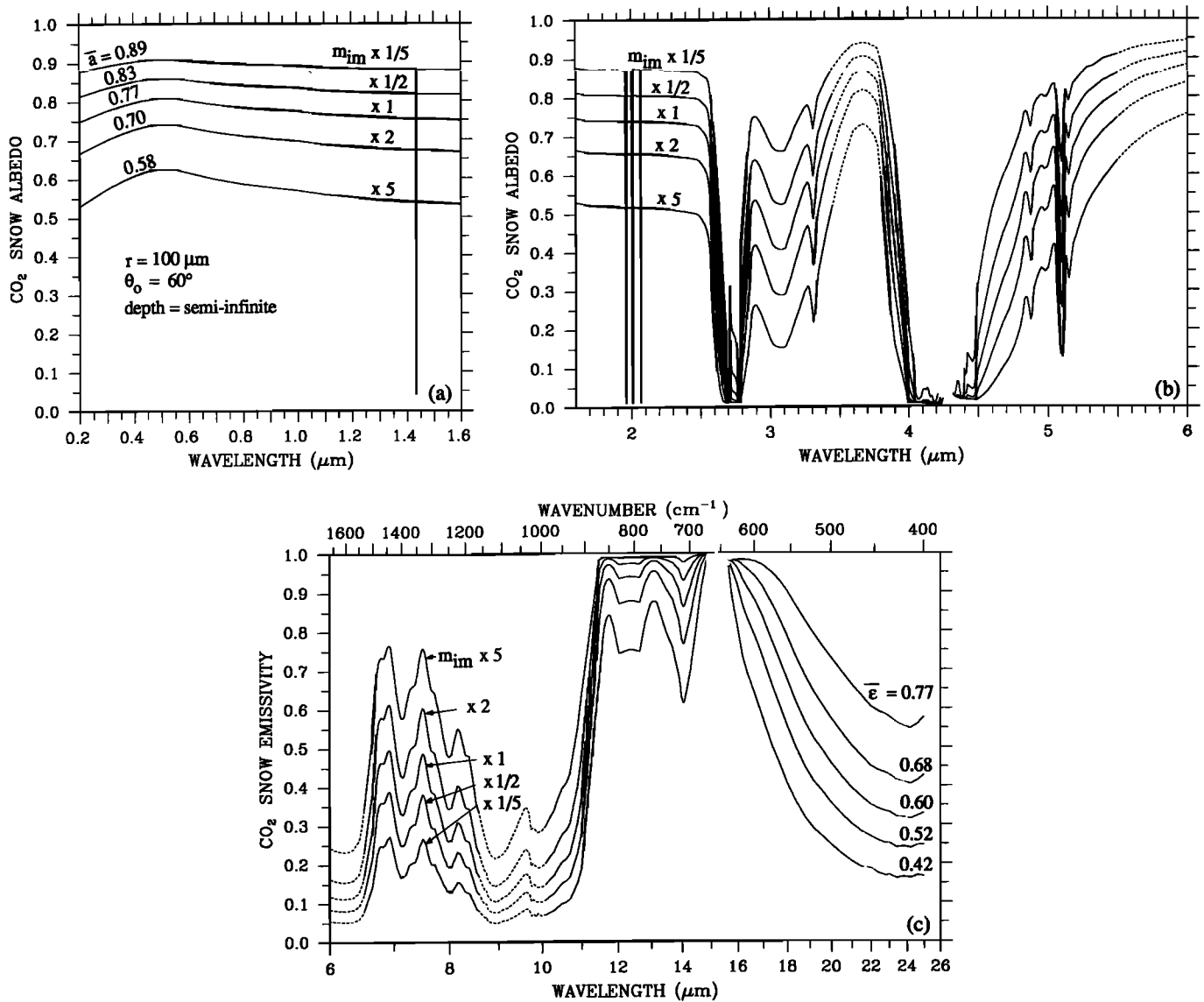


Fig. 18. Sensitivity of CO₂ snow spectral albedo and emissivity to error in imaginary refractive index of pure solid CO₂.

We can offer no new explanation for the large differences in brightness temperature among the four surface-sensing channels in spring and summer over the south polar cap, when these temperatures are higher than the sublimation temperature of CO₂. Addition of water or dust to CO₂ snow, expected in summer, should reduce these interchannel differences, and yet they remain. Kieffer's [1979] idea that unresolved (sub-grid-scale) frost-free regions mix their warm temperatures (and uniform ϵ) together with CO₂ frost (of variable ϵ) in the same pixel seems reasonable.

The role of water is likely to be crucial in determining the energy budget of the polar cap. H₂O is deposited along with CO₂ in the winter but should accumulate as a layer at the surface in spring and summer. The addition of a thin layer of water frost over pure CO₂ snow dramatically raises the thermal emissivity, so that less of the energy balance in spring and summer has to be contributed by latent heat of CO₂ sublimation. A surface cover of water frost of 0.01 g cm⁻² is sufficient to raise the average emissivity to 97%.

Addition of water ice, either within or as a surface

deposit, is unable to raise the spectrally averaged albedo of a CO₂ snowpack (because H₂O snow has low albedo in the near-infrared), unless the underlying CO₂ snow is dirty.

Because of the large uncertainty in the optical constants of solid CO₂ at most wavelengths, our calculations of CO₂ snow albedo and emissivity should be regarded as preliminary suggestions. The detailed infrared spectra of the Martian south pole from Mariner 7 (T. Z. Martin, submitted manuscript 1989) show several features which are likely due to CO₂ but which do not appear in our calculations because of our lack of accurate spectra for pure solid CO₂, especially in the 1.0-2.5 μm region. Calvin [this issue] shows that these Mariner spectra indicate inaccuracies in the optical constants recommended by Warren [1986], in particular that Warren's values are far too low in the 3-4 μm and 5-6 μm regions, by a factor of 10 in some places. We conclude that considerable insight into the climate of Mars could be gained by laboratory experiments on Earth.

Acknowledgments. We thank James Pollack for suggesting (in 1980) that we undertake this study. We are also

grateful to reviewers David Paige and William Smythe for their comments on the initial draft of this paper. We have benefited from several discussions with Hugh Kieffer. Some of the computations were done at the National Center for Atmospheric Research. The work was supported by NSF grants ATM-80-24641 and ATM-86-05134, and NASA grant NAGW-1734.

References

- Bohren, C.F., Applicability of effective-medium theories to problems of scattering and absorption by nonhomogeneous atmospheric particles, *J. Atmos. Sci.*, **43**, 468-475, 1986.
- Bohren, C.F., and D.R. Huffman, *Absorption and Scattering of Light by Small Particles*, 530 pp., Wiley-Interscience, New York, 1983.
- Briggs, G., K. Klaasen, T. Thorpe, and J. Wellman, Martian dynamical phenomena during June-November 1976: Viking orbiter imaging results, *J. Geophys. Res.*, **82**, 4121-4149, 1977.
- Calvin, W.M., Additions and corrections to the absorption coefficients of CO₂ ice: Applications to the Martian south polar cap, *J. Geophys. Res.*, this issue.
- Chylek, P., V. Ramaswamy, and V. Srivastava, Albedo of soot-contaminated snow, *J. Geophys. Res.*, **88**, 10,837-10,843, 1983.
- Clark, R.N., and T.B. McCord, Mars residual north polar cap: Earth-based spectroscopic confirmation of water ice as a major constituent and evidence for hydrated minerals, *J. Geophys. Res.*, **87**, 367-370, 1982.
- Davies, D.W., Effect of dust on the heating of Mars' surface and atmosphere, *J. Geophys. Res.*, **84**, 8289-8293, 1979.
- Davies, D.W., and L.A. Wainio, Measurements of water vapor in Mars' Antarctic, *Icarus*, **45**, 216-230, 1981.
- Davies, D.W., C.B. Farmer, and D.D. LaPorte, Behavior of volatiles in Mars' polar areas: A model incorporating new experimental data, *J. Geophys. Res.*, **82**, 3815-3822, 1977.
- Ditteon, R., and H.H. Kieffer, Optical properties of solid CO₂: Application to Mars, *J. Geophys. Res.*, **84**, 8294-8300, 1979.
- Dobbins, R.A., and G.S. Jizmagian, Optical scattering cross sections for polydispersions of dielectric spheres, *J. Opt. Soc. Am.*, **56**, 1345-1350, 1966.
- Dozier, J., and S.G. Warren, Effect of viewing angle on the infrared brightness temperature of snow, *Water Resour. Res.*, **18**, 1424-1434, 1982.
- Egan, W.G., and F.A. Spagnolo, Complex index of refraction of bulk solid carbon dioxide, *Appl. Opt.*, **8**, 2359-2360, 1969.
- Fink, U., and G.T. Sill, The infrared spectral properties of frozen volatiles, in *Comets*, edited by L.L. Wilkening, pp. 164-202, University of Arizona Press, Tucson, 1982.
- Gaizauskas, V., Studies of the infrared and Raman spectra of gaseous, liquid and solid carbon dioxide, Ph.D. thesis, 64 pp., Univ. of Toronto, Ont., Canada, 1955.
- Gate, L.F., Light-scattering cross sections in dense colloidal suspensions of spherical particles, *J. Opt. Soc. Am.*, **63**, 312-317, 1973.
- Gow, A.J., On the accumulation and seasonal stratification of snow at the south pole, *J. Glaciol.*, **5**, 467-477, 1965.
- Grenfell, T.C., and D.K. Perovich, Radiation absorption coefficients of polycrystalline ice from 400-1400 nm, *J. Geophys. Res.*, **86**, 7447-7450, 1981.
- Grenfell, T.C., D.K. Perovich, and J.A. Ogren, Spectral albedos of an alpine snowpack, *Cold Reg. Sci. Technol.*, **4**, 121-127, 1981.
- Grim, R.E., *Clay Mineralogy*, McGraw-Hill, New York, 1953.
- Haberle, R.M., and B.M. Jakosky, Sublimation and transport of water from the north residual polar cap on Mars, *J. Geophys. Res.*, **95**, 1423-1437, 1990.
- Hansen, J.E., and L.D. Travis, Light scattering in planetary atmospheres, *Space Sci. Rev.*, **16**, 527-610, 1974.
- Hess, S.L., R.M. Henry, and J.E. Tillman, The seasonal variation of atmospheric pressure on Mars as affected by the south polar cap, *J. Geophys. Res.*, **84**, 2923-2927, 1979.
- Hunt, G.E., E.A. Mitchell, H.H. Kieffer, and R. Ditteon, Scattering and absorption properties of CO₂ ice spheres in the region 360-4000 cm⁻¹, *J. Quant. Spectrosc. Radiat. Transfer*, **24**, 141-146, 1980.
- Iversen, J.D., J. B. Pollack, R. Greeley, and B.R. White, Saltation threshold on Mars: The effect of interparticle force, surface roughness, and low atmospheric density, *Icarus*, **29**, 381-393, 1976.
- Jakosky, B.M., Comment on 'Mars residual north polar cap: Earth-based spectroscopic confirmation of water ice as a major constituent and evidence for hydrated minerals' by Roger N. Clark and Thomas B. McCord, *J. Geophys. Res.*, **88**, 4329-4330, 1983.
- Jakosky, B.M., The seasonal cycle of water on Mars, *Space Sci. Rev.*, **41**, 131-200, 1985.
- Jakosky, B.M., and R.M. Haberle, Year-to-year instability of the Mars south polar cap, *J. Geophys. Res.*, **95**, 1359-1365, 1990.
- James, P.B., and G.R. North, The seasonal CO₂ cycle on Mars: An application of an energy-balance climate model, *J. Geophys. Res.*, **87**, 10,271-10,283, 1982.
- James, P.B., G. Briggs, J. Barnes, and A. Spruck, Seasonal recession of Mars' south polar cap as seen by Viking, *J. Geophys. Res.*, **84**, 2889-2922, 1979.
- Joseph, J.H., W.J. Wiscombe, and J.A. Weinman, The delta-Eddington approximation for radiative flux transfer, *J. Atmos. Sci.*, **33**, 2452-2459, 1976.
- Kieffer, H.H., Near infrared spectral reflectance of simulated Martian frosts, Ph.D. thesis, 94 pp., Calif. Inst. of Technol., Pasadena, 1968.
- Kieffer, H., Spectral reflectance of CO₂-H₂O frosts, *J. Geophys. Res.*, **75**, 501-509, 1970.
- Kieffer, H.H., Mars South Polar spring and summer temperatures: A residual CO₂ frost, *J. Geophys. Res.*, **84**, 8263-8288, 1979.
- Kieffer, H.H., H₂O grain size and the amount of dust in Mars' residual north polar cap, *J. Geophys. Res.*, **95**, 1481-1493, 1990.
- Kieffer, H.H., S.C. Chase Jr., E.D. Miner, F.D. Palluconi, G. Münch, G. Neugebauer, and T.Z. Martin, Infrared thermal mapping of the Martian surface and atmosphere: First results, *Science*, **193**, 780-786, 1976.
- Kieffer, H.H., T.Z. Martin, A.R. Peterfreund, and B.M. Jakosky, Thermal and albedo mapping of Mars during the Viking primary mission, *J. Geophys. Res.*, **82**, 4249-4291, 1977.
- Kuhn, M., Die spektrale Transparenz der antarktischen Atmosphäre, Teil II, Messergebnisse und Analyse, *Arch. Meteorol. Geophys. Bioklimatol., Ser. B*, **20**, 299-344, 1972.

- LaChapelle, E.R., Field Guide to Snow Crystals, University of Washington Press, Seattle, 1969.
- Larson, H.P., and U. Fink, Identification of carbon dioxide frost on the Martian polar caps, Astrophys. J., **171**, L91-L95, 1972.
- Lliboutry, L., The origin of penitents, J. Glaciol., **2**, 331-338, 1954.
- Lumme, K., On the surface brightness and geometric albedo of some Martian areas, Icarus, **29**, 69-81, 1976.
- Nussenzweig, H.M., and W.J. Wiscombe, Efficiency factors in Mie scattering, Phys. Rev. Lett., **45**, 1490-1494, 1980.
- Paige, D.A., and A.P. Ingersoll, Annual heat balance of Martian polar caps: Viking observations, Science, **228**, 1160-1168, 1985.
- Pimental, G.C., P.B. Farney, and K.C. Herr, Evidence about hydrate and solid water in the Martian surface from the 1969 Mariner infrared spectrometer, J. Geophys. Res., **79**, 1623-1634, 1974.
- Pollack, J.B., Properties of dust in the Martian atmosphere and its effect on temperature structure, Adv. Space Res., **2(2)**, 45-56, 1982.
- Pollack, J.B., R. Haberle, R. Greeley, and J. Iversen, Estimates of the wind speeds required for particle motion on Mars, Icarus, **29**, 395-417, 1976.
- Pollack, J.B., D. Colburn, R. Kahn, J. Hunter, W. Van Camp, C.E. Carlston, and M.R. Wolf, Properties of aerosols in the Martian atmosphere, as inferred from Viking lander imaging data, J. Geophys. Res., **82**, 4479-4496, 1977.
- Pollack, J.B., D.S. Colburn, F.M. Flasar, R. Kahn, C.E. Carlston, and D. Pidek, Properties and effects of dust particles suspended in the Martian atmosphere, J. Geophys. Res., **84**, 2929-2945, 1979.
- Rhodes, J.J., R.L. Armstrong, and S.G. Warren, Mode of formation of ablation hollows controlled by dirt content of snow, J. Glaciol., **33**, 135-139, 1987.
- Siegel, R., and J.R. Howell, Thermal Radiation Heat Transfer, 862 pp., McGraw-Hill, New York, 1972.
- Singer, R.B., T.B. McCord, and R.N. Clark, Mars surface composition from reflectance spectroscopy: A summary, J. Geophys. Res., **84**, 8415-8426, 1979.
- Smythe, W.D., Spectra of hydrate frosts: Their application to the outer solar system, Icarus, **24**, 421-427, 1975.
- Thomas, P., J. Veverka, and R. Campos-Marquetti, Frost streaks in the south polar cap of Mars, J. Geophys. Res., **84**, 4621-4633, 1979.
- Toon, O.B., J.B. Pollack, and C. Sagan, Physical properties of the particles composing the Martian dust storm of 1971-1972, Icarus, **30**, 663-696, 1977.
- Toon, O.B., J.B. Pollack, W. Ward, J.A. Burns, and K. Bilski, The astronomical theory of climatic change on Mars, Icarus, **44**, 552-607, 1980.
- Wagner, J.K., B.W. Hapke, and E.N. Wells, Atlas of reflectance spectra of terrestrial, lunar, and meteoritic powders and frosts from 92 to 1800 nm, Icarus, **69**, 14-28, 1987.
- Warren, S.G., Optical properties of snow, Rev. Geophys. Space Phys., **20**, 67-89, 1982.
- Warren, S.G., Optical constants of ice from the ultraviolet to the microwave, Appl. Opt., **23**, 1206-1225, 1984.
- Warren, S.G., Optical constants of carbon dioxide ice, Appl. Opt., **25**, 2650-2674, 1986.
- Warren, S.G., T.C. Grenfell, and P.C. Mullen, Optical properties of antarctic snow, Antarct. J. U. S., **21**, 247-248, 1986.
- Warren, S.G., and W.J. Wiscombe, A model for the spectral albedo of snow, II, Snow containing atmospheric aerosols, J. Atmos. Sci., **37**, 2734-2745, 1980.
- Wiscombe, W.J., Improved Mie scattering algorithms, Appl. Opt., **19**, 1505-1509, 1980.
- Wiscombe, W.J., and S.G. Warren, A model for the spectral albedo of snow, I, Pure snow, J. Atmos. Sci., **37**, 2712-2733, 1980.
-
- J. F. Firestone and S. G. Warren, Geophysics Program AK-50, University of Washington, Seattle, WA 98195.
W. J. Wiscombe, Code 613, NASA Goddard Space Flight Center, Greenbelt, MD 20771.

(Received May 8, 1989;
revised November 16, 1989;
accepted November 20, 1989.)